



RESEARCH ARTICLE

10.1002/2014PA002662

Key Points:

- Late Holocene storminess in Bermuda is linked to North Atlantic cooling
- Coastal SSTs in Bermuda are linked to NAO phasing over the late Holocene
- Submarine caves can preserve paleoclimate records

Correspondence to:

P. J. van Hengstum,
vanhenp@tamug.edu

Citation:

van Hengstum, P. J., J. P. Donnelly, A. W. Kingston, B. E. Williams, D. B. Scott, E. G. Reinhardt, S. N. Little, and W. P. Patterson (2015), Low-frequency storminess signal at Bermuda linked to cooling events in the North Atlantic region, *Paleoceanography*, 30, 52–76, doi:10.1002/2014PA002662.

Received 23 APR 2014

Accepted 13 JAN 2015

Accepted article online 15 JAN 2015

Published online 18 FEB 2015

Low-frequency storminess signal at Bermuda linked to cooling events in the North Atlantic region

Peter J. van Hengstum¹, Jeffrey P. Donnelly², Andrew W. Kingston^{3,4}, Bruce E. Williams⁵, David B. Scott⁶, Eduard G. Reinhardt⁷, Shawna N. Little⁶, and William P. Patterson⁴

¹Department of Marine Sciences, Texas A&M University at Galveston, Galveston, Texas, USA, ²Department of Geology and Geophysics, Woods Hole Oceanographic Institution, Woods Hole, Massachusetts, USA, ³Department of Geoscience, University of Calgary, Calgary, Alberta, Canada, ⁴Department of Geological Sciences, University of Saskatchewan, Saskatoon, Saskatchewan, Canada, ⁵Bermuda Institute of Ocean Sciences, St. George's, Bermuda, ⁶Department of Earth Sciences, Dalhousie University, Halifax, Nova Scotia, Canada, ⁷School of Geography and Earth Sciences, McMaster University, Hamilton, Ontario, Canada

Abstract North Atlantic climate archives provide evidence for increased storm activity during the Little Ice Age (150 to 600 calibrated years (cal years) B.P.) and centered at 1700 and 3000 cal years B.P., typically in centennial-scale sedimentary records. Meteorological (tropical versus extratropical storms) and climate forcings of this signal remain poorly understood, although variability in the North Atlantic Oscillation (NAO) or Atlantic Meridional Overturning Circulation (AMOC) are frequently hypothesized to be involved. Here we present records of late Holocene storminess and coastal temperature change from a Bermudian submarine cave that is hydrographically circulated with the coastal ocean. Thermal variability in the cave is documented by stable oxygen isotope values of cave benthic foraminifera, which document a close linkage between regional temperature change and NAO phasing during the late Holocene. However, erosion of terrestrial sediment into the submarine cave provides a “storminess signal” that correlates with higher-latitude storminess archives and broader North Atlantic cooling events. Understanding the driver of this storminess signal will require higher-resolution storm records to disentangle the contribution of tropical versus extratropical cyclones and a better understanding of cyclone activity during hemispheric cooling periods. Most importantly, however, the signal in Bermuda appears more closely correlated with proxy-based evidence for subtle AMOC reductions than NAO phasing.

1. Introduction

Sedimentary evidence from diverse high-latitude coastal environments indicates that a low-frequency storminess signal has persisted across the North Atlantic region through the late Holocene, with events centered during the Little Ice Age (200 to 600 calibrated years (cal years) B.P.), Dark Ages Cold Period (1200 to 1900 cal years B.P. and from 2600 to 3200 cal years B.P.). Evidence includes increased aeolian transport in Iceland [Jackson *et al.*, 2005] and Sweden [de Jong *et al.*, 2006]; coastal sand dune reorganization in the Netherlands [Jelgersma *et al.*, 1995], Ireland [Wilson *et al.*, 2004], and France [Clarke *et al.*, 2002]; terrestrial sedimentary flux into New England lakes [Noren *et al.*, 2002]; estuarine tempestites in France [Sorrel *et al.*, 2009]; and lagoon washover events in the Mediterranean [Sabatier *et al.*, 2012].

Multiple hypotheses have been suggested for how the internal ocean-atmospheric system may be modulating these high-latitude storminess periods. During the Holocene, sea-salt sodium (Na_{ss}) deposition in the Greenland Ice Sheet has been interpreted as a proxy for increased storminess at higher latitudes related to intensified atmospheric circulation-related phasing of the North Atlantic Oscillation (NAO) [e.g., Noren *et al.*, 2002]. However, storminess during the Dark Ages Cold Period (e.g., Iceland [Jackson *et al.*, 2005]) is associated with negligible Na_{ss} accumulation [O'Brien *et al.*, 1995], and recent NAO reconstructions document no salient phase shift at that time [Trouet *et al.*, 2009; Olsen *et al.*, 2012]. Elsewhere, Sabatier *et al.* [2012] observed that storminess in the northwestern Mediterranean is correlated to the 1500 year cycle of ice-rafted debris deposition and cooling in the North Atlantic region [Bond *et al.*, 1997, 2001] and suggested that storminess and decreased AMOC are linked. AMOC variability may also be linked to subpolar gyre circulation dynamics, where contraction of the subpolar gyre causes a southward shift in the westerlies and an increase in the storm tracks over Europe [Thornalley *et al.*, 2009].

Most discussions favor extratropical cyclones as the likely meteorological driver of the North Atlantic low-frequency storminess signal, with little attention given to the possible role of tropical cyclones. However,

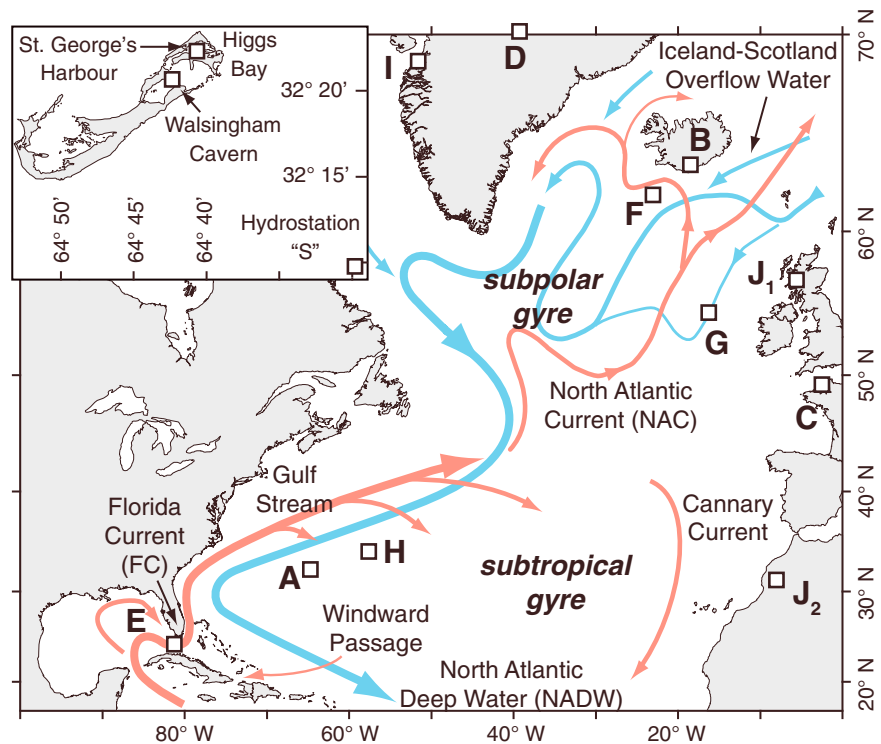


Figure 1. The location of Walsingham Cavern in Bermuda (inset) and in the North Atlantic region (A) compared to Holocene storminess archives from Iceland (B) [Jackson et al., 2005], France (C), and the Greenland Ice Sheet (D) [Dawson et al., 2003]. These sites are placed in a framework of oceanic circulation reconstructions of the Florida Current (E) [Lund et al., 2006], North Atlantic Current (F) [Hall et al., 2004], North Atlantic Deep Water (G) [Oppo et al., 2003], and climate variability in the western subtropical gyre at Bermuda Rise (H) [Keigwin, 1996]. Lastly, North Atlantic Oscillation reconstructions from redox geochemistry in a Greenland lake (I) [Olsen et al., 2012] and another combining a Scottish speleothem (J₁) with Moroccan tree ring data (J₂) in the eastern North Atlantic [Trouet et al., 2009]. The red arrows depict the surface oceanic currents, and the blue arrows depict the oceanic currents at depth.

the impact of tropical cyclones on this signal cannot be ignored because (i) multiple storm types are operant at higher latitudes in the North Atlantic (e.g., tropical storms, tropical cyclones, and extratropical cyclones) and (ii) tropically derived storm systems can even strike Greenland [e.g., Hurricane Erin in 2001], although many first undergo extratropical transition [Jones et al., 2003]. Lower-resolution coastal storminess records often preclude an accurate calibration of sedimentary records to a specific storm type, but they still provide an important perspective of paleotempestology. Two significant questions remain for understanding the North Atlantic low-frequency storminess signal: (1) what is (are) the precise meteorological storm(s) that cause this signal and (2) what climatological mechanisms drive the oscillation?

In the lower latitudes, calibrated sedimentary reconstructions from areas not impacted by extratropical cyclones provide information on tropical cyclone variability through time. In Puerto Rico, intense hurricane activity occurs from 3600 to 4900 cal years B.P., 1000 to 2000 cal years B.P., centered at 500 cal years B.P., and during the last 250 years [Donnelly and Woodruff, 2007]. A period of elevated hurricane activity occurs in the northern Bahamas from 650 to 350 cal years B.P. [van Hengstum et al., 2014]. In the Gulf of Mexico, high-resolution records indicate active hurricane intervals from 1200 to 600 cal years B.P. and from 2800 to 2300 cal years B.P. [Lane et al., 2011], with decreased hurricane intensity and increased frequency, during the Little Ice Age (~600 cal years B.P. to present) [Lane et al., 2011; Brandon et al., 2013]. The southern Caribbean Sea at Lighthouse Reef in Belize also experienced decreased hurricane activity from 600 cal years B.P. to present [Denomee et al., 2014].

The purpose of this study is to evaluate storminess and thermal variability in the coastal regions of Bermuda over the late Holocene, a location in the subtropical North Atlantic Ocean (Figure 1). Bermuda's regional climate is intimately related to NAO phase oscillations, Atlantic Meridional Overturning Circulation (AMOC),

and subtropical gyre circulation mechanics [Keigwin, 1996; Goodkin *et al.*, 2008b; Saenger *et al.*, 2011]. Furthermore, Bermuda experiences tropical, subtropical, and extratropical cyclone activity [Ruprecht *et al.*, 2002; Guichard *et al.*, 2007]; thus, the storminess history at Bermuda has the potential to inform drivers of storminess across the entire North Atlantic. Problematically, extensive post-depositional sediment reworking by bioturbation and wave action has thus far limited the preservation potential of secular marine climate records in Bermudian marine lagoons [Kuhn, 1984; Vollbrecht, 1996].

Here we present a late Holocene storminess and climate record from Bermuda based on costratigraphic signals of terrestrial erosion and oxygen isotopic ratios of benthic foraminifera ($\delta^{18}\text{O}_b$) archived in Walsingham Cavern, a Bermudian submarine cave. Submarine cave environments exhibit a global distribution across Atlantic [Rasmussen and Brett, 1985; Ohtsuka *et al.*, 2002; Ortiz *et al.*, 2009], Pacific [Ohtsuka *et al.*, 2000; Luter *et al.*, 2003; Kano and Kase, 2008], and Mediterranean [Zabala *et al.*, 1989; Airoidi and Cinelli, 1996; Corriero *et al.*, 2001; Surić *et al.*, 2009] coastal carbonate landscapes, and their submerged speleothems have been used in sea level research for decades [Spalding and Matthews, 1972; Richards *et al.*, 1994; Dutton *et al.*, 2009; Surić *et al.*, 2009].

Sediment in submarine caves, however, has only recently received interest from a paleoclimate perspective because these environments are also habitat for carbonate invertebrates (e.g., gastropods, ostracods, and benthic foraminifera) that are suitable for geochemical analysis [Tabuki and Hanai, 1999; Kitamura *et al.*, 2007; Kano and Kase, 2008; Omori *et al.*, 2010; van Hengstum and Scott, 2011]. Perhaps, the most important issue for developing climate records from submarine caves is the degree of circulation between the saline groundwater mass (seawater) in the submarine caves and the adjacent ocean. The saline groundwater flooding a submarine cave can be directly circulated with the coastal ocean through the process of tidal pumping [Smart, 1984; Beddows *et al.*, 2007; Martin *et al.*, 2012], seawater current upwelling within the karst platform [Gilli *et al.*, 1986; Whitaker and Smart, 1990; Moore *et al.*, 1992; Vacelet, 1996], or a combination of both. Most recently, a Japanese team reconstructed 7000 years of paleoceanographic change from oxygen isotopic ratios on bivalves preserved in submarine caves on Okinawa Island [Yamamoto *et al.*, 2008, 2009, 2010], suggesting that submarine cave sediment and microfossils could represent an untapped source of North Atlantic paleoclimate information.

2. Regional Setting

Bermuda is located in the subtropical North Atlantic Ocean in the western Sargasso Sea, where instrumental observations indicate that different oceanographic conditions characterize the open ocean versus the shallow carbonate platform (Figure 1). The open ocean is characterized by a deep mixed layer (>200 m) below a shallow surface layer [Morris *et al.*, 1977; Goodkin *et al.*, 2008a]. Results of temperature monitoring at Hydrostation "S" since 1954 (30 km southeast, 32°10'N, 64°30'W) indicate that sea surface temperatures (SSTs) in the Sargasso Sea ranged from 18.3°C to 28.9°C to a maximum depth of 16 m below sea level, with a mean annual temperature range of 22.4°C to 24.3°C [Goodkin *et al.*, 2008b]. In contrast, Bermuda's shallow coastal waters experience greater seasonality. Monthly SST data recorded in St. George's Harbour (Higgs Bay lagoon, 32°22'13"N, 64°40'40"W) have a maximum range from 15.9°C to 29.8°C, with the mean annual temperatures ranging from 22.8°C to 23.5°C. Thus, long-term temperatures in Bermudian coastal waters and the open ocean are offset, but the greatest offset occurs during the winter when inshore temperatures are on average 2.4°C colder.

Bermudian caves can be generalized as collapsed karst features in a Carbonate Cover Island, according to the Carbonate Island Karst Model [Mylroie and Mylroie, 2007]. This is because Bermuda has a basalt core capped by alternating eolianites and paleosols that developed during late Quaternary sea level highstands and lowstands, respectively [Land *et al.*, 1967; Vacher and Hearty, 1989; Vacher *et al.*, 1995]. Bermudian caves are thought to have formed by three primary processes: vadose dissolution during Quaternary sea level lowstands, further enlargement by phreatic dissolution during Quaternary sea level highstands, and collapse events triggered by loss of buoyant support during regressions [Palmer *et al.*, 1977; Mylroie *et al.*, 1995]. As such, large chambers connected by fissure-collapse tunnels characterize the geometry of most Bermudian caves. Holocene sea level rise has since reflooded many of Bermuda's caves and created diverse underwater cave environments.

Walsingham Cavern has a fissure-like subaerial cave entrance that is located 150 m from the coastline in a pristine subtropical forest (Idwal Hughes Nature Preserve), but it is directly connected to Castle Harbour lagoon by flooded caves (Figure 2). Walsingham Cavern is one large submarine chamber interconnected

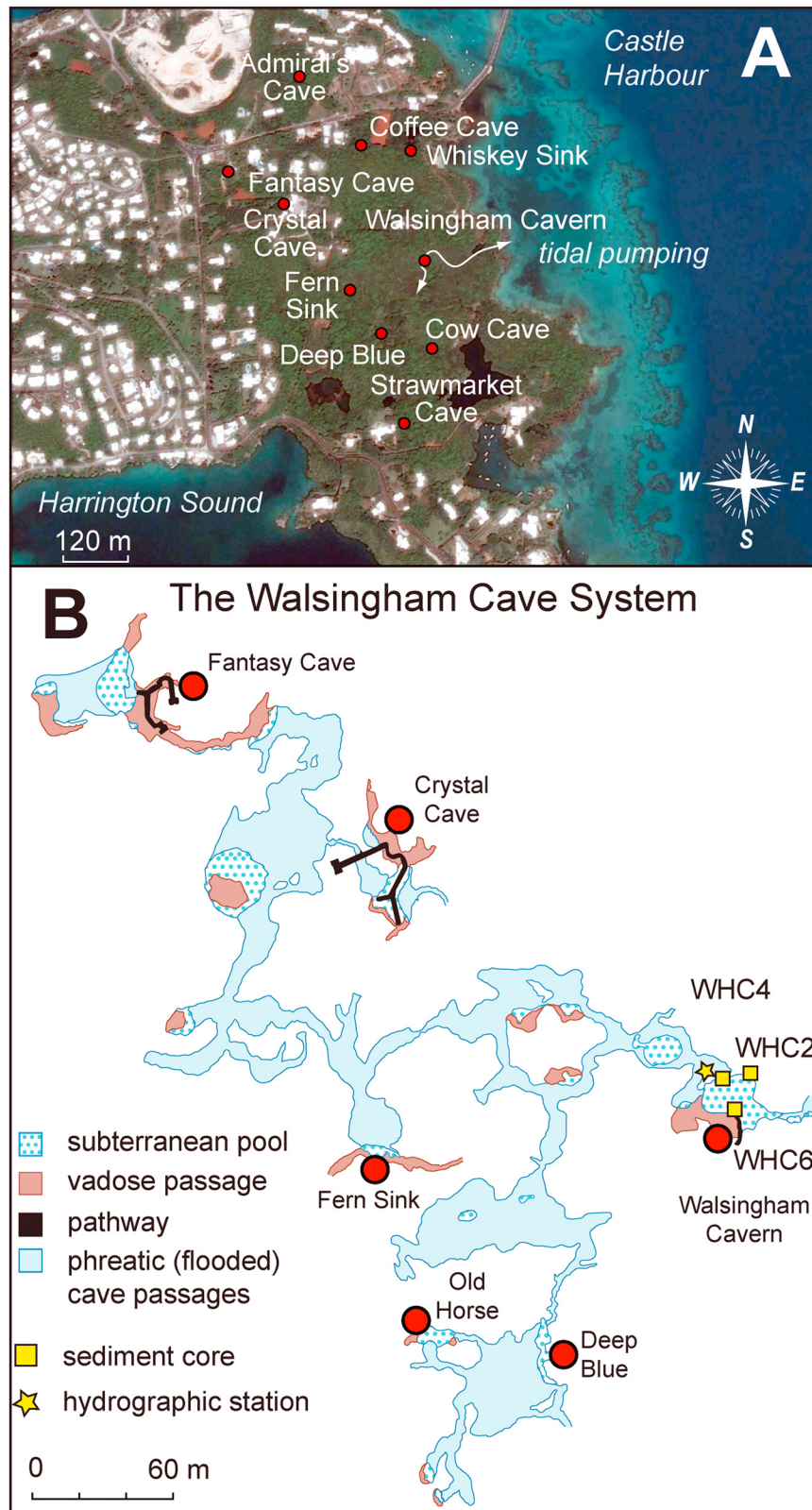


Figure 2. (a) Landsat image of the Idwal Hughs Nature Preserve on Bermuda and the location of several subaerial cave entrances (red circles), many of which are connected by flooded underwater passages into the larger Walsingham Cave System. (b) Detailed cave survey of the Walsingham Cave System with many of the same cave entrances as in top plot (red circles), and the location of sediment cores (yellow squares: WHC2, WHC4, and WHC6) collected in Walsingham Cavern.

within the much larger Walsingham Cave System located on the isthmus between Castle Harbour and Harrington Sound (32°20'53"N, 64°42'37"W; Figure 2). The host lithology for this cave is the Walsingham Formation, which is the oldest and most diagenetically mature Bermudian eolianite with 38% porosity and abundant caves [Land *et al.*, 1967]. The Walsingham Cave System most likely developed over multiple glacioeustatic sea level cycles based on the ubiquity of submerged speleothems but certainly predates the Holocene based on previously dated stalagmites [Harmon *et al.*, 1978].

Groundwater currently flooding Walsingham Cavern is characterized by a thin brackish water cap (meteoric lens, <1 m thick, salinity ~30 practical salinity unit (psu)), buoyed above saline groundwater of full marine salinity [Sket and Illiffe, 1980]. Previous workers have documented the hydrographic connectivity of Walsingham Cavern to the ocean [Sket and Illiffe, 1980; Maddocks and Illiffe, 1986], and exploration by technical cave divers has physically connected Walsingham Cavern to Castle Harbour through a phreatic conduit via Dolphin Pond. Walsingham Cavern itself has minimal tidal current velocities that enable fine carbonate silt to accumulate on the cave floor, and average depth to the sediment-water interface is 18 m below sea level (bsl).

3. Methods

3.1. Cave Hydrography

All sample collections were completed using advanced technical cave scuba diving procedures, while exceeding safety protocols outlined by the American Academy of Underwater Sciences. The scientific dive team acquired extensive training and experience prior to completing the fieldwork described below, as scuba diving in underwater caves is hazardous to untrained personnel. All sampling required swimming materials to, and from, each core site. The sediment cores and hydrographic monitoring station described below were all positioned in the overhead environment.

Saline groundwater temperature was measured in Walsingham Cavern throughout 2010 and 2011 because temperature can be used as a basic proxy for saline groundwater circulation through carbonate platforms [Whitaker and Smart, 1990; Beddows *et al.*, 2005, 2007; Kitamura *et al.*, 2007; Yamamoto *et al.*, 2010]. A thin (<1 m) brackish cap can regionally develop during the wet season [Sket and Illiffe, 1980], so a moored sensor capable of simultaneous temperature and depth measurements was installed into Walsingham Cavern in late 2009 at 8.9 m bsl. This depth ensured that temperature measurements were not influenced by the local meteoric lens, which oscillates 1 to 2 m in elevation from local tidal forcing [Morris *et al.*, 1977]. The hydrographic station continuously autosampled temperature (precision at $\pm 0.01^\circ\text{C}$) and depth (precision at ± 1.2 cm) every 60 s throughout 2010 and 2011, and the resultant data were downloaded every 45 to 60 days to ensure data and battery integrity. Summary statistics (mean, minimum, and maximum) were then calculated from the sum of daily observations (1440 samples).

Cave seawater temperature was then compared to (i) annual SSTs in the Sargasso Sea, (ii) SSTs in St. George's Harbour lagoon at Higgs Bay, and (iii) heat supplied to Bermuda by the Gulf Stream, as estimated by Florida Current transport through the Florida Straits (Figure 1). Sea surface temperature from the Sargasso Sea data was obtained from the Hydrostation "S" program (archived at <http://bats.bios.edu/>), and the 2010 and 2011 temperature measurements from 0 to 75 m bsl were averaged to provide a single SST point to estimate Sargasso Sea thermal variability. For the coastal lagoons, the daily SST measurements from St. George's Harbour were downloaded from the Bermuda weather service (<http://www.weather.bm/>), which are the daily mean of triplicate SST measurements in Higgs Bay. The National Oceanic and Atmospheric Administration's Western Boundary Time Series Project measures the daily volume of the portion of the Florida Current passing through the Florida Straits (± 0.2 sverdrup (Sv)), which can be obtained from http://www.aoml.noaa.gov/phod/floridacurrent/data_access.php.

3.2. Sedimentology

Three push cores were collected from Walsingham Cavern at 18 m bsl in a transect from near the collapse-fissure entrance to inside the cave (Figures 2 and 3). An empty core pipe was first inserted vertically into the sediment to maximum penetration, and the sediment-water interface was subsequently stabilized with a fitted sponge. The pipe was then capped to provide suction for withdrawal of an intact sediment column, and the core sample was subsequently removed from the cave. WHC2 (172 cm and 5 cm diameter) was collected

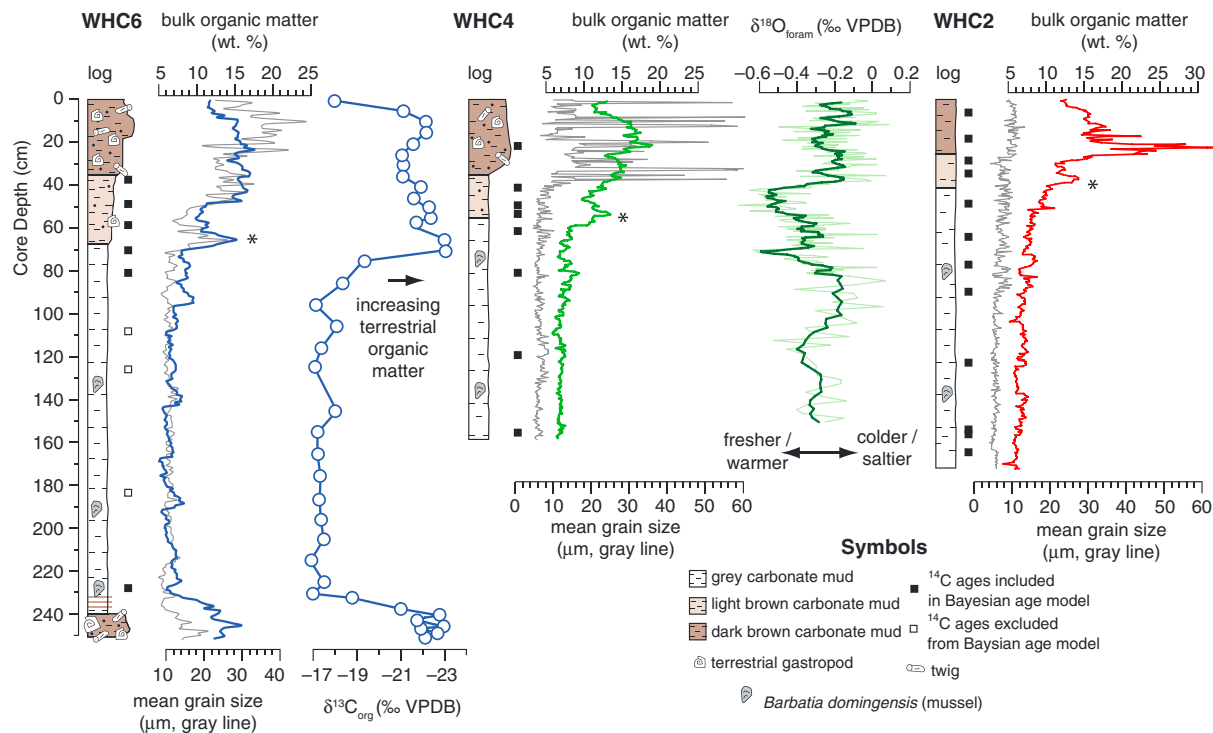


Figure 3. Textural characteristics, isotopic results, and stratigraphic column for each core. Results from WHC6 include the bulk organic matter (wt %, blue line), mean grain size (gray line), and stable carbon isotope values on bulk organic matter ($\delta^{13}C_{org}$). Results from WHC4 include the bulk organic matter (wt %, green line), mean grain size (gray line), and stable oxygen isotope ratios ($\delta^{18}O_f$) on *Triloculina oblonga* (light green line raw data and dark green line is the five-point running mean). Results from WHC2 include bulk organic matter (wt %, red line) and mean grain size (gray line). Note that a significant increase in bulk organic matter occurs at the base of the light brown carbonate mud unit in all cores, which is not necessarily associated with an increase in mean particle size (see asterisk: WHC6: 65 cm, WHC4: 52 cm, and WHC2: 35 cm).

farthest into the cave in 2009, WHC4 (159 cm and 5 cm diameter) collected near the hydrographic station in 2010, and WHC6 (252 cm and 7.6 cm diameter) was collected almost in open water in 2011. The sediment-water interface at this depth is far removed from any influence of the seasonal brackish water cap, as previously described, and is only ever saturated by seawater of open ocean salinity. After collection, core samples were shipped back to the laboratory and preserved moist at 4°C.

Sedimentary texture was examined with laser diffraction particle size analysis with a Beckman Coulter LS230 (precision of $\pm 2 \mu m$ [Eshel et al., 2004]) on bulk (no chemical digestions) subsamples continuously measured downcore every 5 mm. Each subsample was first mechanically disaggregated in a mixture of deionized water and 1% sodium hexametaphosphate using a minivortexor and/or a spatula. Before analysis, particles in each sample were further disaggregated by ultrasonication for 120 s. The efficacy of this procedure at disaggregating and deflocculating sediment particles was further tested because the mean particle sizes for the lower part of WHC2 approached the lower analytical limits of the instrument (4 μm). However, standard deviations on triplicate measurements at 5 cm intervals downcore throughout the entirety of WHC2 ($n = 37$) never exceeded 2 μm , which is the precision of the Beckman Coulter LS230. This extra test demonstrated that the mean particle size measurements obtained by this method are reliable and reproducible, despite the procedure measuring both the organic and carbonate sediment fractions.

Bulk sedimentary organic matter (wt %) was estimated by loss on ignition at 550°C for 4.5 h [Heiri et al., 2001], with typical precision on replicates of $\pm 1\%$. This procedure provided a method to investigate how variations in bulk organic matter have impacted the physical textural measurements. Lastly, the carbon isotope ratio relative to Vienna Peedee belemnite (VPDB) of bulk organic matter ($\delta^{13}C_{org}$) was determined for sediment in the longest core (WHC6) to determine the provenance of the bulk organic matter. Bermudian cave sediments with $\delta^{13}C_{org}$ values higher than -18% are indicative of marine organic matter, and $\delta^{13}C_{org}$ values lower than -24% are indicative of terrestrial organic matter [van Hengstum and Scott, 2011]. For $\delta^{13}C_{org}$ analysis, sediment samples were first digested with 30 mL of 10% HCl to remove carbonate, rinsed to

neutrality, then desiccated and powdered. Subsamples were then introduced into an elemental analyzer coupled to an isotope ratio mass spectrometer to determine $\delta^{13}\text{C}_{\text{org}}$ values to a precision $\pm 0.2\%$.

3.3. $\delta^{18}\text{O}_f$ on *Triloculina Oblonga*

Oxygen isotope values relative to Vienna Peedee belemnite (VPDB) of benthic foraminiferal calcite ($\delta^{18}\text{O}_f$) were measured on *Triloculina oblonga*, which dominates Bermudian submarine caves [van Hengstum and Scott, 2011], to obtain an estimate of hydrographic or thermal variability in Walsingham Cavern through time. Monospecific samples comprising 40 to 50 translucent individuals of *T. oblonga* caught between 90 to 125 μm sized mesh were wet picked for each 5 mm stratigraphic interval. WHC4 was selected for analysis because it was adjacent to the hydrostation. Previous efforts using *Triloculina oblonga* tests that were not specifically translucent produced more ambiguous results [van Hengstum, 2010], perhaps indicating contamination from individuals with secondary shell infillings (e.g., pyrite and possible secondary internal cements). Individual foraminiferal tests from each sample were then transferred into stainless steel cups and roasted in vacuo at 200°C for 1 h to remove water and volatile organic contaminants. Carbonate was then reacted at 70°C with three drops of anhydrous (100%) phosphoric acid for 420 s, and the evolved CO_2 was then cryogenically purified before being passed into a Finnigan Kiel-IV carbonate preparation device directly coupled to a dual-inlet Finnigan MAT 253 isotope ratio mass spectrometer for $\delta^{18}\text{O}$ measurements in the Saskatchewan Isotope Laboratory. Isotope ratios are corrected for acid fractionation and ^{17}O contribution using the Craig correction [Craig, 1957] and then calibrated against internal and national standards (National Bureau of Standards 19) with internal precision on $\delta^{18}\text{O}$ values from replicate samples equal to 0.11‰. Data are reported in standard delta notation (δ) relative to VPDB: $\delta^{18}\text{O}_f = 1000 \times [(^{18}\text{O}/^{16}\text{O})_{\text{sample}} - (^{18}\text{O}/^{16}\text{O})_{\text{standard}}] / (^{18}\text{O}/^{16}\text{O})_{\text{sample}}$. Estimates of the long-term paleotemperature anomaly about the long-term mean were calculated using the temperature equation of Bemis et al. [1998].

3.4. Radiocarbon Dating and Age Models

Twenty-nine accelerated mass spectrometry (AMS) radiocarbon dates provided chronological constraint for the three cores (Table 2). Before analysis, material selected for AMS dating was ultrasonicated to remove any adhering authigenic carbonate particles. All samples were measured by traditional AMS techniques, except for five samples that were dated using the continuous-flow AMS (CFAMS) method developed at the National Ocean Sciences AMS facility [McIntyre et al., 2011; Roberts et al., 2013].

The diverse material dated from WHC2 (benthic foraminifera and ostracods, wood, and bulk sediment) promoted an analysis of reservoir effects on carbonate materials. In WHC2, the conventional ^{14}C age on wood fragments at 154.25 cm is 2600 ± 30 years, whereas the conventional ^{14}C age on benthic foraminifera at 158 to 160 cm is 3260 ± 30 years, which is an apparent 660 year offset (Figure 4a). In fact, all the conventional ^{14}C results from carbonates in WHC2 older than 2600 conventional radiocarbon years appear systematically offset from the two wood samples at 78 and 154 cm (Table 1). This suggests a different ΔR in the lower part of the core (gray carbonate mud) impacted the benthic invertebrates (foraminifera and ostracods), perhaps in response to greater upwelling of saline groundwater through the carbonate, a process observed elsewhere [Gili et al., 1986; Moore et al., 1992; Cordero et al., 2003; Sabatier et al., 2010]. In the upper part of WHC2, however, the carbonate sample from 28 to 30 cm is ~ 130 years older than the wood sample slightly deeper at 33 to 33.5 cm (Table 1). These results suggest a lower ΔR value in the upper part of the core.

This was not the case for the bivalve *Barbatia dominengsis* that was dated in WHC6. This sessile bivalve adheres to the walls of blueholes and ceilings of submarine caves, where it seeks actively circulated water for filter feeding [Logan et al., 1984; Koblunk and Lysenko, 1986], and this species has been successfully used to date similar sites in Bermuda and the Bahamas [van Hengstum et al., 2011, 2014]. It is possible that the life mode of this bivalve isolates the animal from possible old radiocarbon near the sediment-water interface from the advection of saline groundwater through the carbonate lithology below. Multiple calibration and age model permutations from WHC6 demonstrated that a local reservoir correction of ΔR value of -48 ± 40 and Marine13 provided the most appropriate calibration for this bivalve.

Therefore, conventional ^{14}C ages on carbonate benthic invertebrates (foraminifera and ostracods) and bulk organics from WHC4 and WHC2 that were older than 2600 years were calibrated into calendar years before present (cal years B.P.₋₁₉₅₀) using the Marine13 curve and a ΔR value of $+260 \pm 60$ years. Conventional radiocarbon ages from younger benthic invertebrates were calibrated with a local reservoir correction of ΔR

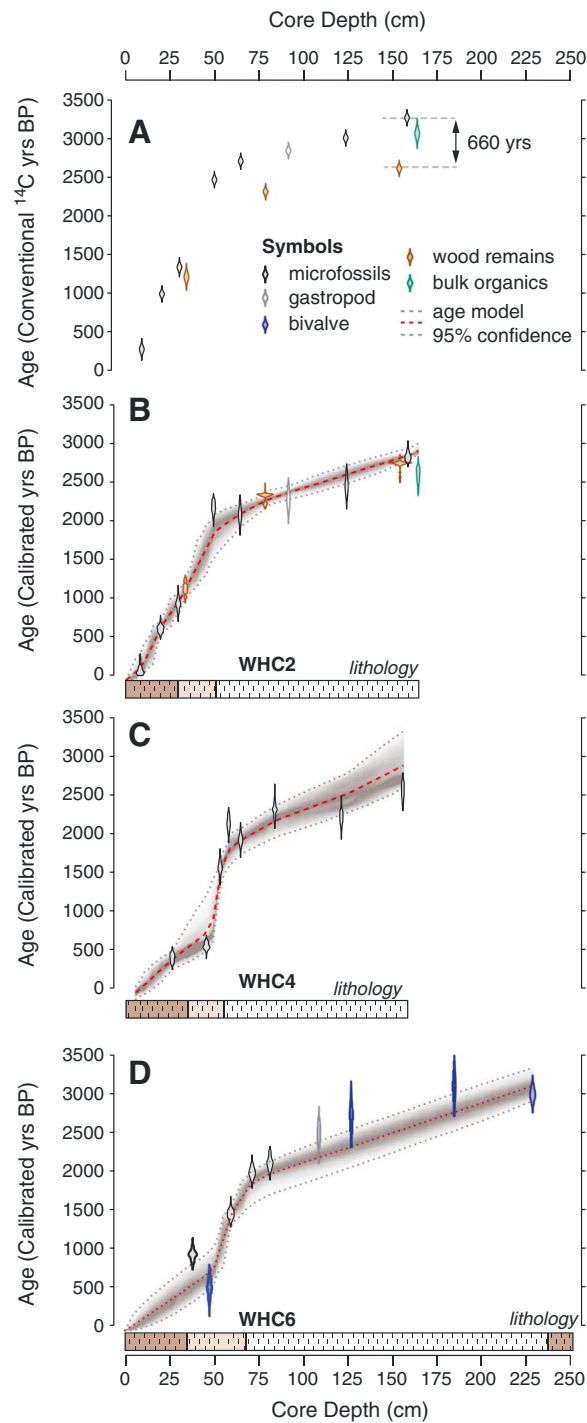


Figure 4. Radiocarbon results for each core. (a) Conventional radiocarbon years for all dates obtained from WHC2. Note that the systematic offset or 260 years between the wood samples (brown) at 33 and 78 cm and carbonate results from adjacent benthic invertebrates, suggesting that older radiocarbon was systematically into the shell structure. (b–d) Bayesian age model for each core calculated with *Bacon* [Blaauw and Christen, 2011], which was constructed using calibrated radiocarbon ages. The symbols for the generalized lithology below each age model are the same as in Figure 3.

value of -48 ± 40 [Druffel, 1997; Reimer et al., 2013]. Conventional ^{14}C ages on wood dates were calibrated into calendar years before present using IntCal13 [Reimer et al., 2013].

A final age model was then constructed for each individual core. The sediment budget throughout Walsingham Cavern is impacted by the proximity of a locale to the subaerial entrance (point source effect, discussed in section 5.1), which necessitates that the sedimentary data in each core be interpreted with respect to its own age model. Age models for each core were generated using a Markov chain Monte Carlo Bayesian statistical approach in the program *Bacon* [Blaauw and Christen, 2011]. Bayesian techniques incorporate stratigraphic ordering into the calibration approach, such that the ages themselves should increase with depth in the core, and they provide a means of assigning downcore uncertainty estimates on time [Blockley et al., 2007, 2008; Bronk Ramsey, 2008]. Calibration of conventional radiocarbon ages into calendar years before present (cal years B.P.₁₉₅₀) was completed in *Bacon* prior to age model generation, and the surface of each core was constrained by the year of collection. All radiocarbon dates from WHC2 and WHC4 were included when generating their final age models (Figures 4b and 4c). However, the radiocarbon date from 38 to 40 cm on WHC6 was excluded from the model for being stratigraphically too old relative to the age at 47 to 47.5 cm. Similarly, the three radiocarbon results generated using the CFAMS technique in the lower part of WHC6 were too old relative to the AMS date at 227.5 to 228.5 cm. However, the full 2σ calibration on these lower CFAMS dates is within 95% confidence interval for the final Bayesian age model generated for WHC6 (Figure 4d), suggesting that the resultant age model for WHC6 is also a good fit for the CFAMS dates.

4. Results

4.1. Seawater Source and Circulation

Walsingham Cavern experienced over 10°C of thermal variability throughout both 2010 and 2011. Minimum temperatures of $\sim 16^\circ\text{C}$ were observed between January and mid-March, and maximum temperatures of $\sim 27^\circ\text{C}$ were observed between late August and late

Table 1. Radiocarbon Results for WHC2, WHC4, and WHC6^a

Index Number	Laboratory Number	Core	Core Depth (cm)	Material Dated	Conventional ¹⁴ C age	δ ¹³ C (‰)	1σ Calibrated Years B.P.1950 (Probability)	2σ Calibrated Years B.P.1950 (Probability)
1	OS-80319	WHC2	6.5 to 8.5	foraminifera	270 ± 40	0.03	<400	<400
2	OS-79182	WHC2	18 to 20	foraminifera	985 ± 30	-0.12	559-645 (1)	521-677 (1)
3	OS-79183	WHC2	28 to 30	foraminifera	1330 ± 35	-0.7	865-992 (1)	789-1046 (1)
4	OS-74181	WHC2	33 to 33.5	wood fragments	1200 ± 50	-21.79	1061-1182 (0.950) 1213-1222 (0.050)	986-1032 (0.090) 1047-1263 (0.910)
5	OS-80319	WHC2	48 to 50	foraminifera	2460 ± 30	0.31	2116-2265 (1)	2035-2305 (1)
6	OS-80296	WHC2	63 to 65	foraminifera	2700 ± 30	0.28	1980-2171 (1)	1920-2280 (1)
7	OS-78405	WHC2	78 to 78.5	wood fragments	2300 ± 30	-27.16	2317-2349 (1)	2184-2235 (0.166) 2305-2355 (0.834)
8	OS-79184	WHC2	91 to 91.5	marine gastropod	2830 ± 30	1.44	2155-2316 (1)	2055-2406 (1)
9	OS-79185	WHC2	123 to 125	foraminifera	3000 ± 30	0.38	2343-2545 (0.967) 2550-2560 (0.033)	2313-2674 (1)
10	OS-78404	WHC2	154 to 154.5	wood fragments	2600 ± 30	-25.6	2734-2755 (1)	2714-2772 (1)
11	OS-80298	WHC2	158 to 160	foraminifera	3260 ± 30	0.85	2714-2842 (1)	2649-2952 (1)
12	OS-74182	WHC2	164 to 165	bulk organics	3050 ± 55	-18.97	2430-2665 (1)	2332-2716 (1)
13	OS-81524	WHC4	20 to 22	foraminifera and ostracods	710 ± 30	-0.19	334-348 (0.098) 352-454 (0.902)	294-485 (1)
14	OS-81446	WHC4	40 to 42	foraminifera	890 ± 30	0	497-567 (0.858) 578-595 (0.142)	473-630 (1)
15	OS-87328	WHC4	48 to 50	foraminifera and ostracods	1950 ± 30	-0.09	1497-1630 (1)	1416-1690 (1)
16	OS-87367	WHC4	53 to 55	foraminifera	2430 ± 35	not measured	2051-2215 (1)	1992-2290 (1)
17	OS-81445	WHC4	60 to 62	foraminifera	2260 ± 30	0.24	1859-1985 (1)	1798-2065 (1)
18	OS-81450	WHC4	80 to 82	foraminifera and ostracods	2580 ± 30	0.4	2246-2390 (1)	2153-2451 (1)
19	OS-87331	WHC4	119 to 121	foraminifera	2810 ± 30	0.87	2142-2302 (1)	2026-2360 (1)
20	OS-87326	WHC4	155 to 157	foraminifera	3080 ± 30	0.93	2482-2683 (1)	2366-2720 (1)
21	OS-97065	WHC6	38 to 40	foraminifera and ostracodes	1320 ± 20	-0.06	862-968 (1)	792-1022 (1)
22	CFAMS	WHC6	47 to 47.5	<i>Barbatia domingensis</i>	830 ± 110	N/A	408-613 (1)	281-664 (1)
23	OS-97066	WHC6	58 to 60	foraminifera and ostracodes	1850 ± 20	-0.56	1391-1505 (1)	1332-1548 (1)
24	OS-97067	WHC6	70 to 72	foraminifera and ostracodes	2310 ± 20	0.25	1916-2043 (1)	1867-2107 (1)
25	OS-97172	WHC6	80 to 82	foraminifera and ostracodes	2410 ± 20	0.37	2025-2171 (1)	1983-2271 (1)
26	CFAMS	WHC6	108.5 to 109	marine gastropod	2990 ± 110	N/A	2320-2618 (0.945) 2622-2643 (0.055)	2141-2737 (1)
27	CFAMS	WHC6	126.5 to 127	<i>Barbatia domingensis</i>	2949 ± 112	N/A	2652-2944 (1)	2433-3075 (1)
28	CFAMS	WHC6	184 to 185	<i>Barbatia domingensis</i>	3250 ± 110	N/A	2984-3294 (1)	2831-3410 (1)
29	Beta-316152	WHC6	227.5 to 228.5	<i>Barbatia domingensis</i>	3150 ± 30	1	2918-3074 (1)	2854-3150 (1)

^aSamples designated by the laboratory number CFAMS were dated using the continuous-flow AMS (CFAMS) method, which do not have accession numbers. All calibrated dates are reported with zero as representing 1950 A.D.

October. Table 1 summarizes the annual temperature variability between Walsingham Cavern, St. George's Harbour lagoon, and the surface mixed layer of the Sargasso Sea. It is also noteworthy that the variation in the mean annual temperature between the three locales is within 1°C. However, the temperature variability in Walsingham Cavern during seasonal and tidal cycles provides further insight into the origin of its seawater.

Tidal pumping of seawater from the lagoons into Walsingham Cavern during the flood tidal cycle appears to be the primary driver of cave temperature change. In the winter of 2010, seawater with a minimum temperature of ~16°C entered the cave at high tide (flood tidal cycle), causing a rapid 4°C cooling in Walsingham Cavern (Figure 5a, blue inset). During the ebb tidal cycle, however, some seawater is entering Walsingham Cavern that circulated through the carbonate platform (in saline groundwater circulation cells [Whitaker and Smart, 1990]) that was originally derived from the surface mixed layer in the Sargasso Sea. In winter 2012, temperature rebounded over the ebb tidal cycle to above 20°C, as seawater warmer than that observed in the lagoon advected through the local karst and into the cave. In opposition to the winter season, summertime high tides (flood tidal cycle) caused a short-lived, time-lagged warming in Walsingham Cavern, while the ebb tidal cycle caused cooling inside the cave (Figure 3a, red insets).

The most likely sources of seawater in Walsingham Cavern are the adjacent lagoon (St. George's Harbour) and the surface mixed layer (upper 75 m) of the Sargasso Sea. Overall, the mean daily temperature inside Walsingham Cavern is highly correlated to SSTs in St. George's Harbour at Higgs Bay (Pearson correlation

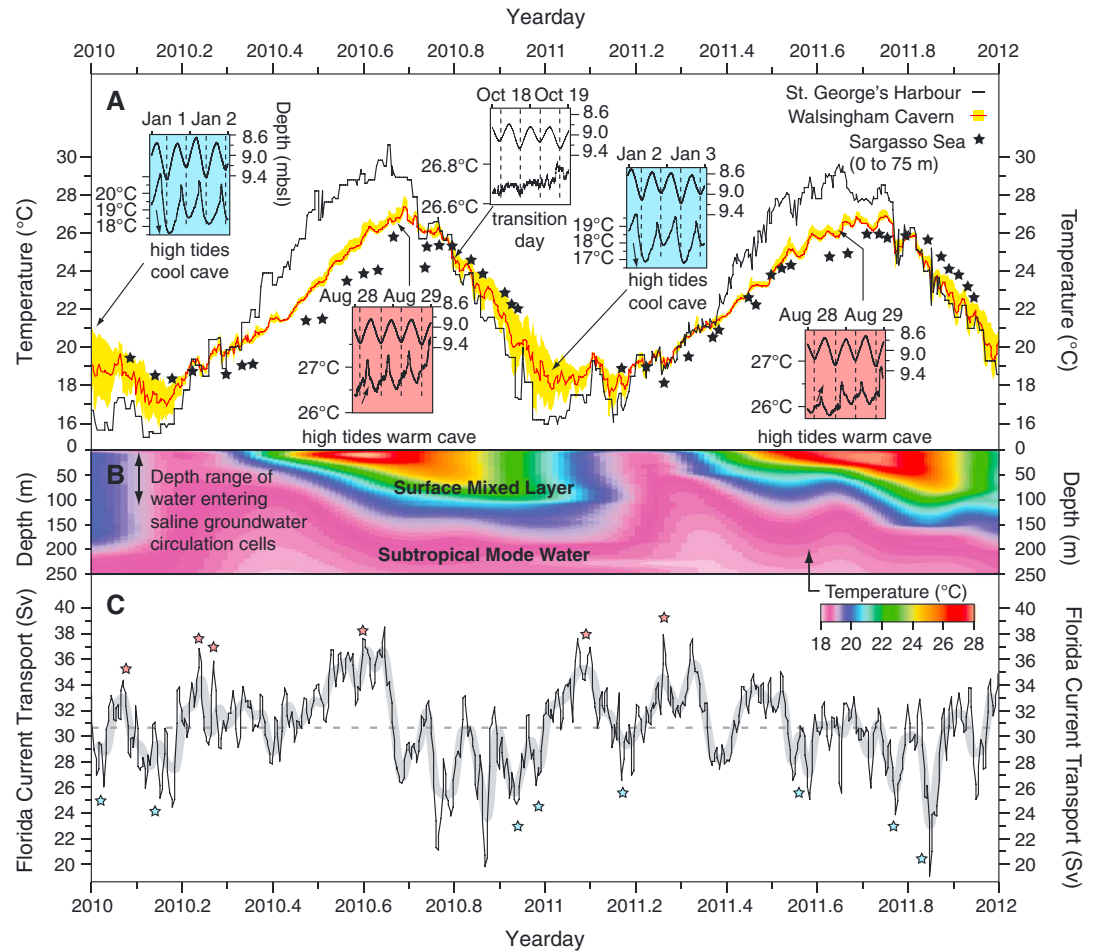


Figure 5. Thermal variability in Walsingham Cavern (2010 and 2011) compared to regional oceanography. (a) Temperature change in Walsingham Cavern (the red line is the daily mean, and the yellow shading is the daily range) compared to sea surface temperature in the Sargasso Sea at Hydrostation S (upper 75 m) and a coastal lagoon (Higgs Bay in St. George's Harbour). The insets illustrate the temperature change during tidal cycles in the winter (blue) and summer (red). Twice a year (late October and mid-March), SSTs align between the coastal lagoons and the upper 75 m of the Sargasso Sea, causing negligible temperature change (less than 0.1°C) in Walsingham Cavern during tidal cycles (white inset labeled "transition day"). In all insets, the sensor is deepest in the water column during high tide. (b) Thermal structure of upper Sargasso Sea at Hydrostation S. (c) Florida Current (FC) transport through the Florida Straits (daily: black; weekly: gray). The Mean Florida Current (FC) transport from 2010 to 2011 was 30.8 ± 3 Sv (dashed line), and the gray line indicates the weekly mean transport. The red (blue) stars denote other events where prominent FC transport changes can be correlated to rapid temperature increases (decreases) in Walsingham Cavern.

coefficient = 0.948, $p < 0.001$), but coastal SSTs alone do not account for the daily temperature variation in Walsingham Cavern associated with the tidal cycle. During the flood tidal cycle, the direct connection of Walsingham Cavern to Castle Harbour permits the influx of seawater into the cave. However, the ebb tidal cycle acts to pull seawater through the porous carbonate into the cavern itself (Figure 5). This process of tidal pumping does not require a physical connection to the ocean [Martin et al., 2012] and has been documented elsewhere with more temporally limited data sets [Beddows et al., 2007]. However, the detailed temperature changes over a tidal cycle in Walsingham Cavern indicates that the most likely source of this secondary water is the surface mixed layer (upper 75 m) of the Sargasso Sea. The upper 75 m of the Sargasso Sea remains warmer (cooler) than the inshore lagoons during the winter (summer), and the ebb tidal cycle reflects seawater temperatures that precisely align with the surface mixed layer in the Sargasso Sea (Table 2).

This hypothesis is supported by the observation that biannually, there is alignment between the temperatures in the lagoon, the surface mixed layer in the Sargasso Sea, and Walsingham Cavern (e.g., 2010.2 and 2011.8). Temperature variability in Walsingham Cavern during these alignment periods was unresolved (approached

Table 2. Mean Monthly Temperature Change in Walsingham Cavern Compared to SST Change in the Coastal Lagoon (Higgs Bay, St. George’s Harbour) and Mean Annual Average Temperature in Walsingham Cavern Compared to SSTs in St. George’s Harbour Lagoon and the Surface Mixed Layer in the Sargasso Sea at Hydrostation “5”

2010 Monthly	Cave Temperatures (°C)			Lagoonal SST (°C)		
	Average	Minimum	Maximum	Average	Minimum	Maximum
January	18.8	18.5	19.7	16.5	17.4	15.7
February	17.7	17.0	18.7	15.9	17.2	15.3
March	18.3	16.9	19.4	17.5	19.4	15.8
April	19.7	18.8	20.5	19.7	20.5	18.5
May	20.9	20.1	21.6	22.4	23.9	19.9
June	22.2	21.4	23.2	25.4	28.2	23.7
July	24.3	23.3	25.2	28.0	28.8	26.7
August	26.1	25.2	26.8	29.4	30.6	28.5
September	26.6	25.9	27.9	27.7	29.1	25.7
October	25.1	23.3	26.5	25.3	26.8	23.3
November	22.7	20.4	24.6	21.8	23.9	19.6
December	19.8	16.5	22.6	17.8	20.0	16.0
2010 Annual	Cave Temperature (°C)		Lagoonal SST (°C)		Sargasso Sea SST (°C)	
Average	21.9		22.3		21.9	
SD	3		4.8		2.5	
Minimum	16.5		15.9		18.4	
Maximum	27.9		29.4		25.8	
2011 Monthly	Cave Temperatures (°C)			Lagoonal SST (°C)		
	Average	Minimum	Maximum	Average	Minimum	Maximum
January	18.3	16.7	19.9	16.7	17.5	16.0
February	18.6	16.5	19.8	17.7	19.3	16.1
March	18.9	17.2	19.9	18.6	19.8	16.7
April	20.0	18.5	21.1	19.9	21.3	18.6
May	21.4	20.8	22.3	21.8	23.8	20.8
June	23.0	22.0	23.8	25.3	27.3	24.1
July	24.7	23.5	25.9	27.6	28.4	26.4
August	26.0	25.5	27.0	28.7	29.6	27.8
September	26.5	26.0	27.2	27.9	28.5	27.5
October	25.6	24.1	27.2	26.0	28.1	24.0
November	23.1	21.1	24.8	22.8	25.2	21.6
December	21.0	18.3	23.1	20.5	22.2	18.6
2011 Annual	Cave Temperature (°C)		Lagoonal SST (°C)		Sargasso Sea SST (°C)	
Average	22.3		22.8		23.3	
SD	2.9		4.2		2.4	
Minimum	16.5		16.7		18.2	
Maximum	27.2		28.7		26.4	

instrumental precision) because SST in both the lagoons and Sargasso Sea created little temperature variability over tidal cycles (Figure 3a, white inset). It appears unlikely that subtropical mode water, which remains constant at 18°C [Schroeder et al., 1959], is the secondary source of seawater entering Walsingham Cavern because one would expect mode water to leave a thermally consistent fingerprint during the ebb tidal cycle over the annual cycle (Figure 5b). Therefore, Walsingham Cavern is diurnally circulated with seawater primarily derived from Castle Harbour and secondarily circulated with water from the surface mixed layer from the Sargasso Sea (Figure 6).

The daily and intraseasonal thermal variability in Walsingham Cavern further indicate the control of regional climate on cave seawater temperature. Temperature change in Walsingham Cavern is correlated with Florida Current transport, where an ~1°C temperature increase (decrease) in Walsingham Cavern can be associated with a 2 to 3 Sv increase (decrease) in Florida Current transport (Figure 3c). Over the winter season from January to mid-March in 2010 and 2011, temperature change in Walsingham Cavern was significantly correlated to both Florida Current transport through the Florida Straits (Pearson correlation coefficient = 0.412, $p < 0.001$) and NAO phasing (Pearson correlation coefficient = 0.322, $p < 0.001$). In fact, there are multiple instances where an increase (decrease) in Florida Current transport are followed by a short-term (3 to 5 days) warming (cooling)

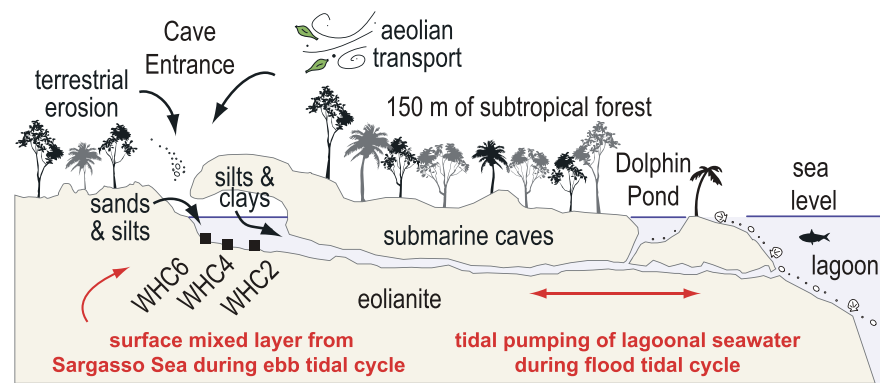


Figure 6. A conceptual model illustrating the point source effect in Walsingham Cavern, where terrestrial sediment enters the subaerial fissure-collapse entrance in the subtropical forest (Idwals Nature Preserve) and is laterally transported into the cave. Temperature monitoring in Walsingham Cavern from 2010 to 2011 indicates that tidal pumping causes seawater to primarily enter the submarine cave from the adjacent lagoon (Castle Harbour). Some seawater, however, is advecting into the submarine cave through the karst that is derived from the upper 75 m of the Sargasso Sea.

trends in Walsingham throughout the biennial record (Figure 5c), albeit with a time delay of a couple days between the Florida Straits and Walsingham Cavern. For example, at 2010.5, an increase of ~ 3 Sv caused an $\sim 1^\circ\text{C}$ increase in temperature in Walsingham Cavern, and a decrease of ~ 3 Sv of Florida Current transport at 2010.2 caused an $\sim 1^\circ\text{C}$ decrease in temperature. This relationship is more challenging to observe in the summer when the seasonal increase in heat from solar radiation far exceeds any possible heat variability supplied to the Bermudian region by Florida Current transport variations. The rapid hourly, tidal, and seasonal temperature changes in Walsingham Cavern in response to ocean, atmospheric, and solar forcings indicate that Walsingham Cavern is a hydrographically open system that is well circulated with Bermuda's regional oceans.

4.2. Chronology and Sedimentation

All three cores recovered stratigraphy containing three primary sedimentary units dating back to at least ~ 3100 calibrated years before present (cal years B.P.): a topmost dark brown carbonate mud, a light brown carbonate mud, and a gray carbonate mud (Figure 3). These stratigraphic changes are neither anthropogenic nor related to sea level because Bermuda was uninhabited until 1609 A.D. and relative sea level in Bermuda has changed minimally during the late Holocene, respectively [van Hengstum *et al.*, 2011]. Natural forest changes are also unlikely as *Juniperus* dominated the Bermudian landscape since the mid-Holocene, with declines since colonization (1609 A.D.) related to anthropogenic activities [Watts and Hansen, 1986; Rueger and von Wallmenich, 1996].

WHC6 penetrated the deepest of all cores and sampled an older dark brown carbonate mud unit (230 to 250 cm) that was not collected in the shorter WHC2 and WHC4 (Figure 3). In WHC6, the basal dark brown carbonate mud was deposited prior to 2900 cal years B.P. (Figure 4d) and contained coarser particles ($13 \pm 1 \mu\text{m}$, medium silt) and higher bulk organic matter ($15 \pm 3\%$) relative to the other two sedimentary units. Most importantly, this unit contained terrestrial material such as twig fragments and the Bermudian endemic terrestrial gastropod *Poecilozonites*, similar to the topmost dark brown carbonate mud unit observed in all cores. The $\delta^{13}\text{C}_{\text{org}}$ values were lower than -23‰ below 230 cm in WHC6 (Figure 3), which suggests that the bulk organic matter is primarily terrestrial material.

At ~ 3100 cal years B.P., the dark brown carbonate unit in WHC6 passes into a thick sequence (1.5 m) of gray carbonate mud, which was also recovered in WHC2 and WHC4. Based on the age model from WHC2 and WHC6, the gray carbonate mud unit was deposited from ~ 3000 to ~ 1700 cal years B.P. (mean age model 2σ result: WHC6: 1720 ± 180 , WHC4: 1760 ± 180 , and WHC2: 1500 ± 290 cal years BP). The gray carbonate mud was the finest grained unit recovered (silt, mean $5\text{--}8 \mu\text{m}$) and was characterized by the least bulk organic matter content relative to the other two units (mean $\sim 7\%$). The $\delta^{13}\text{C}_{\text{org}}$ values on the bulk organic matter were higher than -18‰ , which indicates that marine constituents primarily comprise the bulk organic matter. Walsingham Cavern also experienced the highest sedimentation rates of the late Holocene during the deposition of the gray carbonate mud ($\sim 1 \text{ mm yr}^{-1}$).

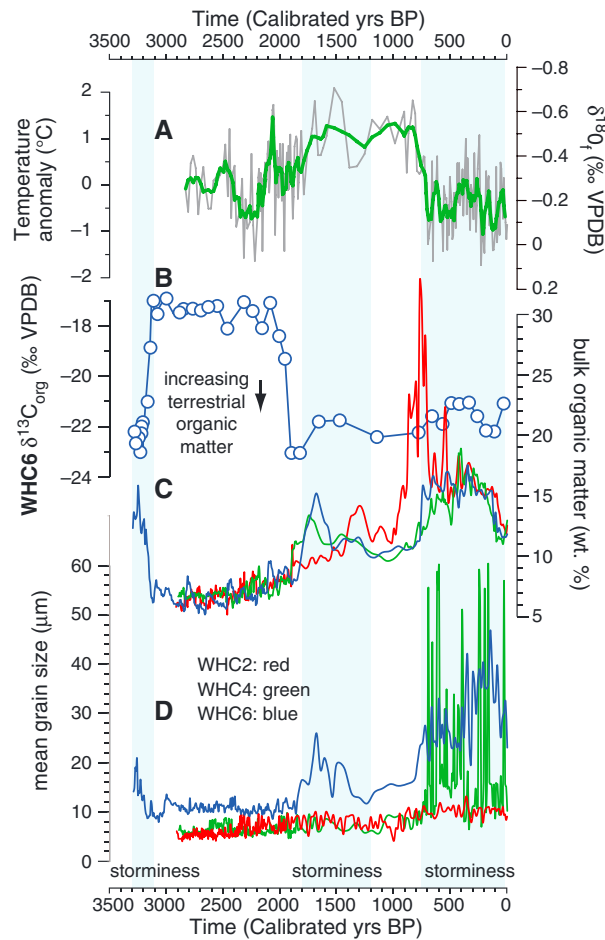


Figure 7. Sedimentary and isotopic results plotted against time using the individual Bayesian age models for each core. (a) The $\delta^{18}O_f$ results (light gray) and five-point running mean (green line) from *T. oblonga* in WHC4, plotted on same axis as the estimated temperature anomaly using the temperature equation of Bemis *et al.* [1998]. (b) The $\delta^{13}C_{org}$ results from WHC6, where more negative isotopic ratios indicate greater proportion of terrestrial material in the bulk organic matter deposited into the cave. (c) Bulk organic matter (wt %) in each core. (d) Mean particle size in each core. The three salient intervals where bulk organic matter and particle size increase represent increased deposition of terrestrial material in response to regional storminess (blue bars): the Little Ice Age from 100 to 600 cal years B.P., the Dark Ages Cold Period from 1300 to 1800 cal years B.P., and prior to 3100 cal years B.P. Data in this figure are color coded (WHC2: red, WHC4: green, and WHC6: blue).

the light brown carbonate mud. Given the small size of the system, however, this early increase in bulk organic matter in WHC2 is most likely stratigraphically continuous with the increase bulk organic matter in WHC4 and WHC6. Negligible particle size variability is ever observed in WHC2, but a rapid particle size increase does occur in WHC4 and WHC6 that exceeds $30 \mu m$ (coarse silt), with deposition during some intervals exceeding the sand-sized fraction ($>63 \mu m$).

4.3. Integrity of $\delta^{18}O$ Results

The $\delta^{18}O_f$ values are useful for estimating paleotemperature changes if the oxygen isotope value of seawater ($\delta^{18}O_{sw}$) is known because there is temperature-dependent fractionation between water and calcite, resulting in a 0.2‰ increase in $\delta^{18}O_f$ for every $1^\circ C$ decrease in temperature [Kim and O'Neil, 1997; Bemis *et al.*, 1998].

In all cores, the gray carbonate mud transitions to a light brown carbonate mud from ~ 1700 to 600 cal years B.P., coinciding with the lowest sedimentation rates observed in the late Holocene (0.1 to 0.2 mm yr^{-1}). These low sedimentation rates limit the temporal resolution of any paleoclimate reconstructions during the accumulation of this sedimentary unit. This unit contains more bulk organic matter than the gray carbonate mud ($10\text{--}13\%$). It is noteworthy that a significant increase (i.e., peak) in bulk organic matter occurs at the base of this unit in all cores but not necessarily an increase in mean particle size (see the asterisk in Figure 3 on WHC6: 65 cm, WHC4: 52 cm, and WHC2: 35 cm), which is outside the analytical uncertainty for the method. The $\delta^{13}C_{org}$ values for this unit in WHC6 are -23‰ , suggesting that the organic matter provenance was the adjacent terrestrial environment. Little particle size variability is observed at WHC2 or WHC4 at the onset of this unit, but mean particle size markedly increases from $12 \mu m$ to $26 \mu m$ at the base of the unit in WHC6 (73 cm; Figure 3), which is the core most proximal to the subaerial entrance.

The topmost unit in all cores was a dark brown carbonate mud that began deposition at ~ 700 cal years B.P. (mean age model 2σ result: WHC6: 540 ± 250 , WHC4: 592 ± 290 , and WHC2: 840 ± 170 cal years B.P.). This unit has the highest bulk organic matter of all cores, which is primarily terrestrial material based on $\delta^{13}C_{org}$ values around -22‰ . *Poecilozonites* and terrestrial plant fragments were again observed in the unit, similar to the basal dark brown carbonate mud unit in WHC6. In WHC2, the increase in bulk organic matter in WHC2 appears to predate the increase in bulk organic matter in WHC4 and WHC2 by ~ 100 years (Figure 7), but this may be a relict of low sedimentation rates in

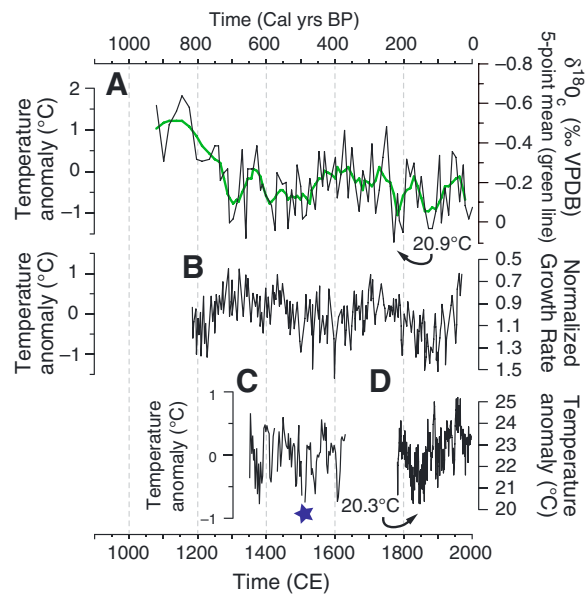


Figure 8. (a) Thermal variability in Walsingham Cavern over the last millennium estimated from *T. oblonga* shells. The age model on this reconstruction has no less than 200 year uncertainty throughout this interval (95% confidence interval). The green line is the five-point running mean, where the raw data appear as back. (b) A coral temperature reconstruction from skeletal extension rates of a long-lived *Monastrea cavernosa* [Pätzold et al., 1999]. This is a digitized version of the original data set, which has never been publically released. Temperature reconstructions from shorter-lived *D. labyrinthiformis* corals provide comparative data from (c) 600 to 400 years ago [Draschba et al., 2000] and over (d) the last 200 years [Goodkin et al., 2008b]. The star denotes a suspected interval of coastal cooling that caused coral growth cessation [Draschba et al., 2000].

an open system, where the cave seawater is sourced from, and actively circulated with, the Sargasso Sea and coastal lagoons (section 4.1). These locations are the habitat of the previously analyzed planktonic foraminifera and corals, respectively. Even after considering the limitations imposed by potentially variable $\delta^{18}\text{O}_{\text{sw}}$ values through time, $\delta^{18}\text{O}_f$ values from *Triloculina oblonga* should provide a first-order test of any possible thermal variability in Walsingham Cavern.

Temperature estimates from core-top $\delta^{18}\text{O}_f$ values are consistent with the recent seawater temperatures measured in Walsingham Cavern. The $\delta^{18}\text{O}_f$ value of the topmost sample in WHC4 (0 to 0.5 mm) was 0.09‰, which provides a temperature estimate of 21.8°C. Furthermore, three samples from the top 1.5 cm of WHC4 have a mean $\delta^{18}\text{O}_f$ value on 134 *T. oblonga* shells of -0.08‰ that provide a temperature estimate of $21.7 \pm 0.3^\circ\text{C}$. This very closely approximates the mean annual temperature we measured in Walsingham Cavern for 2010 A.D. (21.9°C) and 2011 A.D. (22.3°C). Based on these results, it appears that $\delta^{18}\text{O}_f$ measurements on smaller *T. oblonga* can be used to estimate mean thermal variability in Walsingham Cavern.

Coral growth rates provide an additional test of the $\delta^{18}\text{O}_f$ results because Bermudian coral growth is inversely correlated to sea surface temperature [Dodge and Vaišnyš, 1975; Logan et al., 1994]. Figure 8b coplots an 800 year reconstruction of coastal SST in Bermuda based on extension rates of a *Monastrea cavernosa* coral. A $+0.5^\circ\text{C}$ warming trend occurs from 775 to 575 cal years B.P. is followed by cooler temperatures from 500 to 375 cal years B.P. Afterward, a 1°C warming centered at 350 cal years B.P. is followed by the lowest temperatures observed in the late nineteenth century [Pätzold et al., 1999]. Results from Walsingham Cavern suggest two prominent -1.0°C cooling trends (800 to 500 cal years B.P. and 200 cal years B.P. to present), interrupted by a warmer interval with a return to mean conditions centered at 400 cal years B.P. Statistical

However, the straightforward use of $\delta^{18}\text{O}_f$ values in paleothermometry is hampered because $\delta^{18}\text{O}_{\text{sw}}$ values also vary linearly with salinity [Bemis et al., 1998; Katz et al., 2010]. At Bermuda, however, $\delta^{18}\text{O}_f$ values from planktonic foraminifera and coral are a reliable proxy for late Holocene paleotemperature because local climate change significantly alters local seawater temperature to robustly impact $\delta^{18}\text{O}_f$ values relative to $\delta^{18}\text{O}_{\text{sw}}$ [Keigwin, 1996; Draschba et al., 2000; Kuhnert et al., 2005; Goodkin et al., 2008a]. During the instrumental period, the annual average surface salinity variability at Hydrostation “S” has been less than 0.3 psu, and coral reconstructions actually indicate fresher surface waters during the Little Ice Age (LIA) at Bermuda that would act to create pseudowarmer paleotemperature estimates from $\delta^{18}\text{O}_c$ values [Goodkin et al., 2008a]. As such, the $\delta^{18}\text{O}$ ratios from foraminiferal and coral carbonate in the Bermudian region have been repeatedly used to evaluate long-term thermal variability related to North Atlantic climate change [Keigwin, 1996; Draschba et al., 2000; Kuhnert et al., 2005; Goodkin et al., 2008a] and corroborate the $\sim 1^\circ\text{C}$ cooling observed elsewhere throughout the North Atlantic [Keigwin, 1996].

Long-term salinity information for Walsingham Cavern is unknown. However, the available hydrographic measurements indicate that it is

comparisons between the coral and cave reconstructions are inappropriate because there is no less than 200 years of temporal uncertainty in the age model (95% confidence interval), which increases below 26 cm in the core (or 650 cal years B.P.) when sedimentation rates diminish. However, the overall trends between Walsingham Cavern and the *M. cavernosa* coral are very similar in magnitude over the last 200 years but appear phase shifted at ~100 years older prior to 400 cal years B.P. This is possibly because the date used in the age model for WHC4 at 48 to 50 cm is from within the light brown carbonate unit, a period characterized by the lowest sedimentation rates of the late Holocene, as previously discussed. Despite these possible uncertainties, nevertheless, the long-term thermal trends between the corals and Walsingham Cavern are grossly consistent.

Two additional SST reconstructions based on *D. labyrinthiformis* corals further document Bermudian SST variability. The lowest temperatures of the last 200 years occur in the mid-1800s (20.3°C) according to a SST reconstruction by Goodkin *et al.* [2008a, Figure 8d], which is within the uncertainty of the coldest temperature recorded in Walsingham Cavern at 1773 A.D. (20.9°C). A partial SST reconstruction from another *D. labyrinthiformis* coral that lived from 640 to 370 cal years B.P. largely replicates the *M. cavernosa* SST trends [Draschba *et al.*, 2000], but a growth interruption in the *D. labyrinthiformis* at ~490 cal years B.P. suggests that local conditions may have been too cold for coral growth (Figure 8c, see blue star). This growth interruption occurs during the cooling trend in Walsingham Cavern from 500 to 600 cal years BP.

Walsingham Cavern does not document the warming trend of the last 30 years documented by the *M. cavernosa* or *D. labyrinthiformis* coral, suggesting that the upper centimeters of WHC4 may have been lost or homogenized through the coring process on scuba. However, the overall similarities between thermal trends in Walsingham Cavern and coral-based SST reconstructions introduce confidence for using the measured $\delta^{18}\text{O}_f$ values to estimate late Holocene SST variability in coastal Bermuda (Figure 10b). However, this investigation does lack a thorough examination of modern salinity variation, so the discussion of the $\delta^{18}\text{O}_f$ results is constrained to the long-term change in the temperature anomaly.

5. Discussion

5.1. Cave Sediment Budget and Source

The sediment budget in Walsingham Cavern includes inputs from three primary sources over the late Holocene: (1) autochthonous marine biologic constituents (carbonate and organic) from benthic productivity (e.g., foraminifera, ostracods, bryozoans, and marine algae), (2) inorganic autochthonous carbonate mud production, and (3) allochthonous terrestrial sediment. The two most significant variables impacting sedimentation were the proximity of the core site to the subaerial cave entrance (a point source effect) and a significant reduction in authigenic carbonate precipitation at ~2000 cal years B.P.

Deepest into the cave at WHC2, only fine-grained sediment (4–13 μm) accumulated throughout the late Holocene. However, terrestrial organic matter deposition increased notably during the LIA and centered at 1400 cal years B.P. These results suggest that coarse-grained terrestrial organic sediment was deposited elsewhere in the cave, but the more buoyant terrestrial organic fines were transported deeper into the cave as suspended load. At the site most proximal to the subaerial entrance (WHC6), increased deposition of coarse-grained particles (mean particle size exceeding 15 μm) and bulk organic matter (exceeding 15%) occurred three times: prior to 3100 cal years B.P., from 1800 to 1300 cal years B.P., and during the LIA (Figure 7). Furthermore, particles deposited during the LIA ($30 \pm 7 \mu\text{m}$) were coarser than from 1800 to 1300 cal years B.P. ($18 \pm 3 \mu\text{m}$) and prior to 3100 cal years B.P. ($15 \pm 3 \mu\text{m}$). These results suggest that the most intense particle transport dynamics of the late Holocene occurred during the LIA. At the critical middle site of WHC4, however, particle size increased only during the LIA ($20 \pm 15 \mu\text{m}$), but bulk organic matter deposition first increased at 1600 cal years B.P., then again during the LIA (Figure 6).

The simplest interpretation for the deposition of increased particle sizes and terrestrial organic matter is a varied flux of sediment entering the cave through a point source, in response to recurrent erosion on the Bermudian landscape prior to 3100 cal years B.P., from 1800 to 1300 cal years B.P., and from 700 to 100 cal years B.P. (Figure 10a). Palynological studies do not suggest recurrent local drought [Watts and Hansen, 1986; Rueger and von Wallmenich, 1996; Rueger, 2006], so gross precipitation variability appears insufficient for driving these terrestrial erosion cycles. Surge associated with hurricanes and other storms often transports

coarse-grained allochthonous sediment into otherwise quiescent coastal environments, thereby preserving a characteristic coarse-grained overwash layer in the stratigraphic record [Donnelly *et al.*, 2001; Horton *et al.*, 2009; Park, 2012]. Clearly, another mechanism is transporting sediment in Walsingham Cavern as no classic hurricane overwash layers of marine sediment were observed.

In contrast, high winds or precipitation from storms can dislodge, erode, and mobilize terrestrial sediment particles on the subaerial landscape and transport them into Walsingham Cavern through a point source (i.e., subaerial entrance). The point source effect has been previously observed in Mexican [van Hengstum *et al.*, 2009], Bermudian [van Hengstum *et al.*, 2011], and Bahamian [Cunliffe, 1985] underwater caves and manifests in two primary ways: (1) the preferential deposition of terrestrial sediment near subaerial entrances to underwater caves and (2) the attenuation in sedimentary particle size with increasing distance into underwater caves [van Hengstum *et al.*, 2015]. Bermuda is regularly hit by subtropical, tropical, and extratropical cyclones [Guichard *et al.*, 2007], which can provide the necessary energy for mobilizing particles on the terrestrial landscape. Despite the cores being spatially located ~15 m apart, the sediment entering Walsingham Cavern is clearly laterally sorted, where coarsest particles and most organic matter is deposited proximal to the fissure-collapse entrance, with finer organic matter particles having the greatest potential for becoming transported deeper into the cave (Figure 3). Tidal hydrodynamics would most likely have an equal impact on sedimentation at all core sites, by sorting the sediment or winnowing away fines.

Lateral sorting of sediment in Walsingham Cavern provides some evidence that storminess during the LIA at Bermuda was more intense relative to the 1500 cal years B.P. event. Varying either the frequency or intensity of storms could potentially increase the volume or rate of terrestrial sediment entering Walsingham Cavern, so neither particle size changes nor bulk organic content at a solitary core site can resolve storm specificity, frequency, or intensity. However, the linear positioning of the cores into the cave indicate that coarser terrestrial particles were deposited at WHC4 and WHC6 during the LIA relative to the 1500 cal years B.P. event, and only storminess during the LIA promoted an increase in bulk organic matter deposition farthest into the cave at WHC2 (Figure 7). These results suggest that more intense storms more forcefully transported particles into the cave during the LIA relative to the 1500 cal years B.P. event. Unfortunately, similar comparisons for the >3000 cal years B.P. event cannot be made as the event is only represented in one core (WHC6).

The other significant change to the sediment budget is an abrupt decrease in carbonate mud production at the transition from the gray carbonate mud to the light gray carbonate mud. This is accompanied by a decrease in marine benthic productivity, which is documented by the shift in $\delta^{13}\text{C}_{\text{org}}$ values from above -18‰ to below -23‰ in WHC6 (Figure 7) that indicate a loss of autochthonous marine organics in the system. Perhaps, increased upwelling of saline groundwater through the carbonate platform prior to 2000 cal years B.P. provided more favorable seawater for authigenic carbonate mud production and marine benthic productivity. Increased upwelling could also have caused the different ΔR value in Walsingham Cavern deeper into the record. After 2000 cal years B.P. in the light brown carbonate mud unit, however, benthic invertebrates (e.g., foraminifera and ostracodes) still remain important constituents contributing to the local sediment production, but their size is notably smaller. These processes resulted in a continuous but low sedimentation rate until the LIA when the terrestrial sedimentary flux into Walsingham Cavern increased.

5.2. Bermudian Thermal Variability

Over the last millennium, $\delta^{18}\text{O}_f$ values from Walsingham Cavern suggest that Bermuda's coastal region cooled at ~700 cal years B.P. (Figure 8a), which is within the dating uncertainties of the LIA onset and ~1°C cooling throughout the North Atlantic region [Morberg *et al.*, 2005]. With respect to salinity, geochemical results from the *D. labyrinthiformis* coral indicate that Bermudian inshore waters were fresher during the LIA [Goodkin *et al.*, 2008a], forcing lower regional $\delta^{18}\text{O}_{\text{sw}}$ values. However, $\delta^{18}\text{O}_f$ values from Walsingham Cavern increase relative to long-term values. These competing geochemical factors reiterate that a robust cooling trend occurred in Bermuda during the LIA. As discussed by others [Lund and Curry, 2004; Cronin *et al.*, 2010; Saenger *et al.*, 2011], however, marine thermal variability in the western North Atlantic is complex and zonally variable.

The cooling trend in Bermudian coastal waters centered around 500 cal years B.P. differs from coeval SSTs on the Bermuda Rise at 680 km to the northeast. However, different ocean and atmospheric variables may be driving temperature variability at these two different sites. Decreased CaCO_3 deposition on the Bermuda Rise

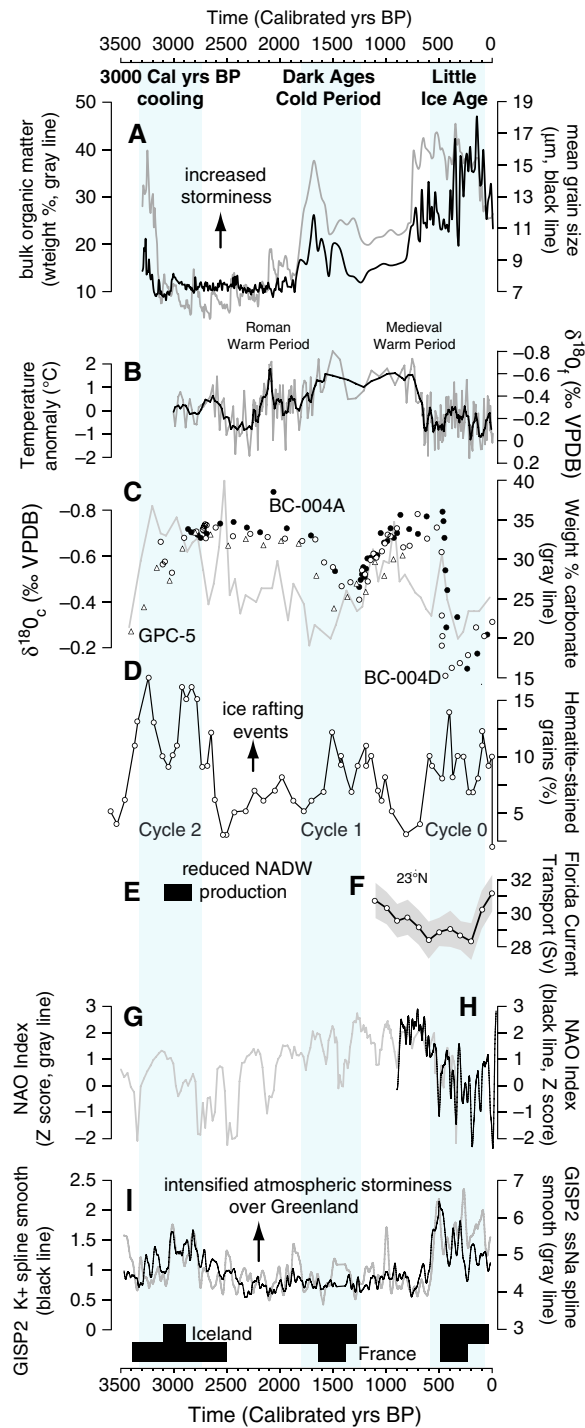


Figure 9

Walsingham Cavern. It is also noteworthy that the Bermuda Rise does not record a significant thermal warming coincident with the Roman Warm Period at 2.1 ka like Walsingham Cavern and Iceland [Patterson et al., 2010], which is another region whose coastal temperature is quite sensitive to NAO variability.

Over the late Holocene, thermal variability in Walsingham Cavern is well correlated with proxy-based evidence for NAO phase oscillations, similar to coral reconstructions [Kuhnert et al., 2005; Goodkin et al., 2008b]. Walsingham Cavern cools abruptly by ~1°C from 700 to 100 cal years B.P., which is within uncertainties

provides evidence for climatic cooling [Keigwin and Jones, 1994], and a robust decrease in CaCO₃ deposition occurs after 500 cal years B.P. (Figure 9c) suggests regional cooling [Keigwin, 1996]. However, the more detailed δ¹⁸O_c-based SST reconstruction from the same Bermuda Rise cores documents two thermal peaks at 900 and 500 cal years B.P. (Figure 9c) that are followed by lower temperature intervals. SST changes at Bermuda Rise have since been correlated with flow velocity of Iceland-Scotland Overflow Water, the precursor to North Atlantic Deep Water, at Björn Drift in the south Iceland Basin [Bianchi and McCave, 1999]. This suggests that the Bermuda Rise SST reconstruction may be indicative of heat transported to this area as driven by AMOC variability. This interpretation is supported by a reduction in Florida Current transport through the Florida Straits at 800 cal years B.P. [Lund et al., 2006] and cooling on Bermuda Rise soon after [Keigwin, 1996]. Furthermore, a short-lived increase in Florida Current transport that occurred around 400 cal years B.P. that was most noticeable in the upper 100 m coincides with the SST increase at 450 cal years B.P. on Bermuda Rise (Figure 9f). These correlations suggest a link between Bermuda Rise SST and heat transport to the North Atlantic, perhaps in response to AMOC variability.

In contrast, SSTs in Bermudian inshore waters are intimately related to NAO variability. Given that the primary source of seawater in Walsingham Cavern is Castle Harbour lagoon, it is unsurprising that there was a strong correlation between the NAO index and wintertime thermal variability in Walsingham Cavern during 2010 and 2011 (see section 4.1). This relationship has also been persistent for several centuries [Goodkin et al., 2008b], whereby NAO⁻ (NAO⁺) decrease (increase) regional SSTs. These results suggest that thermal variability in Walsingham Cavern over millennial time scales would be more sensitive to NAO-like variability than possible AMOC changes, perhaps explaining the SST differences between Bermuda Rise and

of a shift to a long-term NAO⁻ based on proxy evidence from Moroccan tree rings and a Scottish speleothem [Trouet *et al.*, 2009]. NAO forcing also controls redox conditions in a Greenland lake [Olsen *et al.*, 2012], which document a NAO⁻ at the beginning of the LIA and centered at 2400 cal years B.P. (Figure 9g). It is noteworthy that no significant cooling occurs in Walsingham Cavern from 1400 to 1600 cal years B.P. Cooling at Bermuda Rise does occur during this period [Keigwin, 1996], along with increased deposition of hematite-stained grains (cycle 1) in the high latitudes [Bond *et al.*, 2001], but a NAO⁻ was not documented at this time by either Greenland lake geochemistry [Olsen *et al.*, 2012] (Figure 9g) or Na_{ss} deposition in the Greenland Ice Sheet (Figure 9i), a proxy for intensified high-latitude atmospheric circulation processes thought related to NAO phasing [O'Brien *et al.*, 1995]. In fact, the Greenland lacustrine NAO reconstruction suggests an NAO⁺ from ~1900 to 600 cal years B.P. [Olsen *et al.*, 2012]. These results reiterate the important control of NAO phasing on temperature change in Bermudian coastal waters.

These results are significant for understanding the low-frequency storminess signal observed throughout higher latitudes in the North Atlantic [Noren *et al.*, 2002; Sorrel *et al.*, 2009; Sabatier *et al.*, 2012; Sorrel *et al.*, 2012]. NAO-AO-like atmospheric variability is hypothesized as playing a primary role in driving the widely observed North Atlantic higher-latitude storminess signal, so it follows that low-frequency storminess patterns in Bermuda should be closely related to NAO variability, similar to inshore SST variability. However, storminess at Bermuda does not exhibit a simple correlation with evidence for NAO-like variability over the late Holocene, which suggests that more complex ocean-atmospheric dynamics are driving the low-frequency North Atlantic storminess signal.

5.3. Meteorological Drivers of Terrestrial Erosion

In comparison with higher latitudes, the three storminess periods documented in Walsingham Cavern (prior to 3100 cal years B.P., 1300 to 1800 cal years B.P., and 100 to 700 cal years B.P.) are coincident with evidence for increased storminess in the North Atlantic region during the Little Ice Age (200 to 600 cal years B.P.), Dark Ages Cold Period (1200 to 1900 cal years B.P.), and from 3200 to 2600 cal years B.P. Evidence includes increased aeolian transport in Iceland [Jackson *et al.*, 2005] and Sweden [de Jong *et al.*, 2006]; coastal sand dune reorganization in the Netherlands [Jelgersma *et al.*, 1995], Ireland [Wilson *et al.*, 2004], and France [Clarke *et al.*, 2002]; and estuarine tempestites in France [Sorrel *et al.*, 2009]. The results from Walsingham Cavern indicate that the ocean-atmospheric drivers of this low-frequency storminess signal are also operant in the subtropics, a region where tropical cyclones are common.

Both tropical and extratropical cyclones have the potential to impact coastal stratigraphy north of ~30°N, where extratropical cyclones become operant in addition to hurricanes. For example, western Europe receives cyclones of both tropical and extratropical origins, the former often undergoing extratropical transition before reaching Europe [Jones *et al.*, 2003]. The surge and elevated wave climate from both storms can reorganize coastal sediments and so disentangling the storm mechanism responsible for coastal sediment mobilization remains challenging. The exception remains where confining arguments can be made based on favorable geography (e.g., tropics and western Mediterranean coastlines), geomorphology (e.g., barrier overwash requirements), or storm-calibrated high-resolution sedimentary records [Donnelly *et al.*, 2001; Donnelly and Woodruff, 2007; Lane *et al.*, 2011; Sabatier *et al.*, 2012; Brandon *et al.*, 2013]. For example, Pierre Blanch lagoon in the northwestern Mediterranean Sea is not impacted by any storms originating from the deep tropics, yet lagoonal washover events are concentrated during the same low-frequency signal as storminess in Bermuda [Sabatier *et al.*, 2012]. Typical wind speeds of extratropical cyclones seldom rival major hurricanes, but the most vigorous storms often develop during the winter and produce damaging levels of precipitation, hurricane-force

Figure 9. The shaded blue bars demarcating prominent intervals of cooling in the North Atlantic compared to North Atlantic paleoceanographic and paleoclimatic records. (a) Evidence for storminess in Bermuda at Walsingham Cavern as recorded in WHC6 (mean grain size: black line and bulk organic matter: gray line). (b) Oxygen isotope ratios and temperature reconstruction in Walsingham Cavern based on *T. oblonga* tests from core WHC4. (c) Weight percent carbonate and oxygen isotopic ratios on planktonic foraminifera in Bermuda Rise sediment cores [Keigwin, 1996]. (d) North Atlantic ice-rafted debris from higher latitude sediment cores and noted Bond Cycles [Bond *et al.*, 2001]. (e) Prominent interval of reduced North Atlantic Deep Water formation [Oppo *et al.*, 2003]. (f) Florida Current transport reduction during the Little Ice Age, with 95% confidence limit in gray [Lund *et al.*, 2006]. (g) NAO index reconstruction based on redox chemistry in a Greenland lake [Olsen *et al.*, 2012]. (h) NAO index reconstruction from eastern based on a Scottish speleothem and Moroccan tree rings [Trouet *et al.*, 2009]. (i) Sea-salt Na⁺ deposition in the Greenland Ice Sheet Project 2 core [O'Brien *et al.*, 1995]. The bars above the lower abscissa represent the storminess periods in France [Sorrel *et al.*, 2009] and Iceland [Jackson *et al.*, 2005].

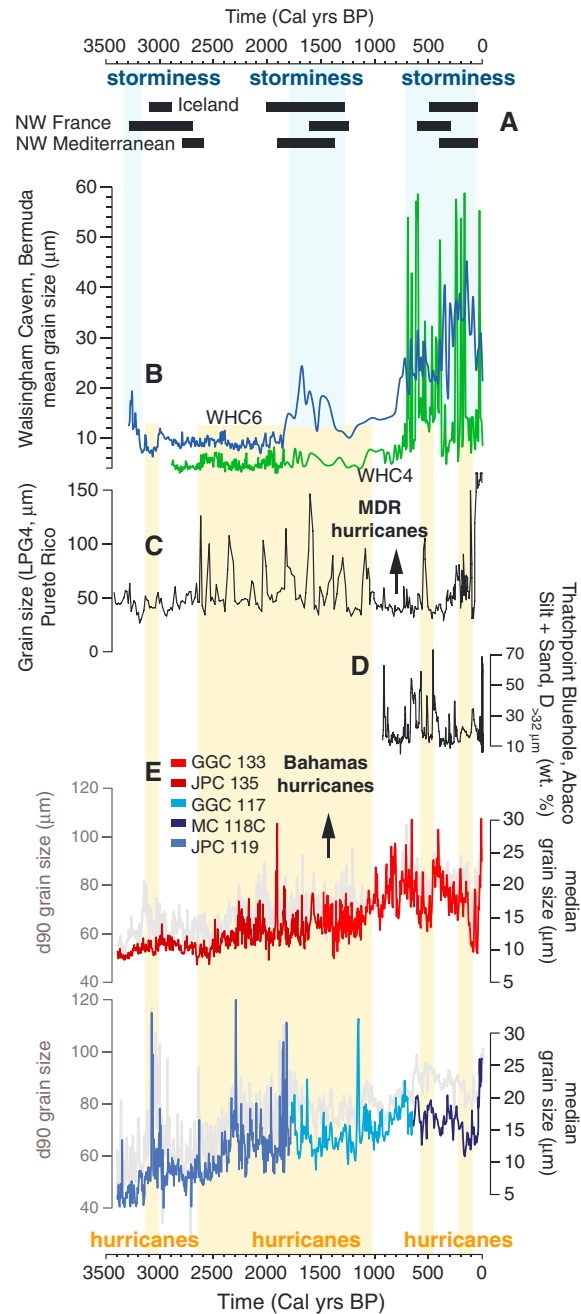


Figure 10

the Great Bahama Bank, which are most likely related to intense hurricane activity [Toomey et al., 2013]. In fact, the entire period of increased terrestrial input into Walsingham Cavern from 1400 to 1900 cal years B.P. coincides with elevated intense hurricane activity in Puerto Rico (Figure 10). If just the coarse fraction anomalies exceeding the high threshold are attributed to hurricane strikes at Mullet Pond [see Lane et al., 2011, Figure 7b], then a decrease in Gulf of Mexico hurricane activity occurred during the Dark Ages Cold Period. Perhaps, evidence for increased storminess in Bermuda during the LIA is related to increased hurricane activity on the northeastern seaboard, where the climate system is favoring a shift in storminess to the northeast. For example, increased tropical cyclogenesis on the northeastern seaboard and their subsequent tracking to higher latitudes can be enhanced during a negative phase of the Atlantic Meridional Mode [Kossin et al., 2010].

winds, and coastal flooding. In fact, extratropical cyclone Lothar (1999) remains one of France's most devastating natural disaster. This suggests that the database of higher-latitude storminess signals are at least in part impacted by extratropical cyclone activity [Sabatier et al., 2012; Sorrel et al., 2012], and so similarly timed elevated extratropical cyclone activity may also have been operating in the Bermuda region. However, tropically derived systems can strike southern Greenland (e.g., 2001, 1993, and 1891 A.D.), suggesting that hurricane may be an important lurking variable impacting North Atlantic higher-latitude "storminess" signals. Disentangling the impact of tropical from extratropical storms on the low-frequency storminess signal observed at higher latitudes is a challenge.

In the lower latitudes, Atlantic hurricane reconstructions can help inform when elevated terrestrial erosion in Bermuda may be related to increased hurricane activity. Storminess in Bermuda appears consistent with evidence for hurricane activity on the northeastern American seaboard but not in the Gulf of Mexico [Lane et al., 2011] or lowest Caribbean latitudes [Denomee et al., 2014]. During the LIA, the double-peaked coarse particle size event observed in both WHC4 and WHC6 centered on 500 and 250 cal years B.P. is strikingly coincident with intense hurricane activity in Puerto Rico [Donnelly and Woodruff, 2007] and the Bahamas [Toomey et al., 2013; van Hengstum et al., 2014]. However, hurricane activity at Lighthouse Reef in Belize decreases at 600 cal years B.P. [Denomee et al., 2014], with evidence suggesting that hurricane intensity and frequency of hurricane in the northeastern Gulf of Mexico decreased ~600 cal years B.P. [Lane et al., 2011; Brandon et al., 2013].

During the Dark Ages Cold Period, the coarse-grained peaks in WHC6 at 1900 cal years B.P. are also coeval with events of increased coarse-grained banktop sediment export from

Furthermore, it remains puzzling why there is little evidence for enhanced terrestrial erosion from 2800 to 2000 cal years B.P. in Bermuda, when surely both tropical and extratropical systems were operant. In the tropics, intense hurricane activity remains elevated during this time interval [Donnelly and Woodruff, 2007]. Perhaps the climate system favored conditions that deviated tropically derived systems from striking Bermuda at this time, simultaneous with the reduced strikes of extratropical systems. An alternative hypothesis would be a reduced frequency or intensity of general storm activity. The lateral sorting of sediments in Walsingham Cavern suggests higher storm energetics during the LIA relative to at 1700 cal years B.P., yet it remains challenging to argue that hurricanes were somehow less capable of transporting terrestrial sediment at 1700 cal years B.P. Furthermore, the slightly elevated SSTs over the Bermuda Rise from 2800 to 2000 cal years B.P. [Keigwin, 1996] should also be enhancing local hurricane activity at this time. As with higher latitudes, additional high-resolution and calibrated records of storm activity will be needed from Bermuda to further disentangle the role of tropical versus extratropical cyclones on the low-frequency storminess signal recorded in Walsingham Cavern.

5.4. Low-Frequency Storminess and North Atlantic Cooling Events

Determining the climatic forcing of these terrestrial erosion intervals in Bermuda is challenging because the exact storm mechanism driving the erosion remains uncertain (tropical versus extratropical storms). However, it is noteworthy that the storminess intervals in Bermuda are not consistently linked to proxy-based evidence for NAO phasing. In the modern system, instrumental observations indicate that positive NAO phases (NAO^+) concentrate winter storms north of $55^\circ N$, whereas negative NAO phases (NAO^-) evenly distribute cyclone tracks to below $40^\circ N$ [Ruprecht et al., 2002; Andrade et al., 2008; Hurrell and Deser, 2009]. However, total North Atlantic and western European extratropical cyclone counts are not completely explained by NAO variability alone [Mailier et al., 2006]. Indeed, increased storminess during the LIA and at >3100 cal years B.P. coincides with proxy evidence for NAO^- in Bermuda (Figure 9), but the correlation is inconsistent at multiple other intervals in the late Holocene. For example, storminess centered at 1500 cal years B.P. coincides with a NAO^+ , and NAO^- at 2100 and 2400 cal years B.P. are not correlated to increased storminess.

In contrast, the three storminess intervals in Walsingham Cavern are all coincident with periods of centennial-scale cooling (~ 0.5 to $1^\circ C$) in the North Atlantic region [Mayewski et al., 2004]. These periods of climatic deterioration and change have been recorded in a variety of proxy archives, such as high-latitude glacier advances [Denton and Karlén, 1973], increased deposition of hematite-stained quartz and feldspar grains in the North Atlantic high latitude [Bond et al., 2001] (Figure 9d), cooling in the subtropical North Atlantic [deMenocal et al., 2000] and reduced $CaCO_3$ deposition on Bermuda Rise (Figure 9c) [Keigwin, 1996], and stratigraphic and moisture changes recorded in European peat bogs [Mauquoy et al., 2002; Swindles et al., 2007; van Geel et al., 2014]. It has been suggested that these periods of climatic cooling are linked to subtle reductions in AMOC, perhaps in response to reduced solar irradiance [van Geel et al., 2000; Bond et al., 2001] or internal climate variability [Renssen et al., 2007]. For example, The most prominent AMOC reduction during the late Holocene occurred at ~ 2800 cal years B.P. [Oppo et al., 2003; Hall et al., 2004] (Figure 9e), and all three intervals of climate cooling coincide with evidence for reduced flow intensity of Iceland-Scotland Overflow Water [Bianchi and McCave, 1999; Hall et al., 2004].

Some evidence suggests that both tropical and extratropical cyclone activity can be linked to AMOC variability. Modeling results from Shaffrey and Sutton [2006] indicate that an amplified (reduced) AMOC decreases (increases) meridional temperature gradients and atmospheric baroclinicity, which in turn can then reduce (increase) extratropical cyclogenesis. Perhaps, this partly explains the correlation between

Figure 10. A comparison between storminess at Bermuda and evidence for increased storminess in the higher latitudes (blue columns) and hurricane activity at lower latitudes along the North American seaboard (yellow columns). (a) Evidence for increased storminess in Iceland [Jackson et al., 2005], the northwestern Mediterranean [Sabatier et al., 2012], and northwestern France [Sorrel et al., 2009]. (b) Mean particle size deposition at WHC4 (green line) and WHC6 (blue line) in Walsingham Cavern, which serve as proxies for storminess at Bermuda. (c) Evidence for elevated hurricane activity at Puerto Rico, which has a scale truncated at $>160 \mu m$ [Donnelly and Woodruff, 2007]. (d) Evidence for elevated hurricane activity at Thatchpoint Bluehole, the Bahamas [van Hengstum et al., 2014]. (e) Coarse-grained sediment deposition on the margin of the Great Bahama Bank as a proxy for storm-mediated sedimentary export off the banktop [Toomey et al., 2013]. The Walsingham Cavern storminess signal coincides with evidence for intervals of both intense tropical [Donnelly and Woodruff, 2007] and extratropical [Sabatier et al., 2012] cyclone activities. MDR: Main Development Region.

Bermudian storminess and paleoceanographic evidence for AMOC variability over the late Holocene, assuming that extratropical cyclone activity at least partly impacts the Walsingham Cavern storminess signal. Furthermore, AMOC variability appears also linked to Atlantic hurricane activity on the American Eastern Seaboard, which could impact storminess in Bermuda. Latitudinal changes in the Intertropical Convergence Zone, in response to either internal or external forcing, can alter wind stress curl over the North Atlantic subtropical gyre, in turn altering oceanic heat transport [Lund *et al.*, 2006], and tropical cyclone genesis on the American Eastern Seaboard [Donnelly *et al.*, 2015]. Therefore, it remains possible that the North Atlantic low-frequency storminess signal is actually the net result of dynamic changes to both tropical and extratropical storm dynamics during late Holocene hemispheric cooling events. Problematically, little analog for such a climate state exists during the instrumental period.

6. Conclusions

This study presents an innovative costratigraphic record of temperature and storminess from a submarine cave in Bermuda (Walsingham Cavern) to help understand the low-frequency storminess signal that persists in North Atlantic paleoclimate records. Bermuda's regional climate is strongly linked to modern NAO variability, and since NAO-like atmospheric variability is thought to be significantly involved with the Holocene North Atlantic storm signal, the storminess history at Bermuda may significantly inform North Atlantic storm dynamics. Walsingham Cavern in Bermuda is hydrographically circulated with the coastal lagoon through the process of tidal pumping, which means that internal carbonate microfossils observe regional oceanographic change. In addition, Walsingham Cavern also has a subaerial opening ~150 m from the coastline in a subtropical forest, serving as a conduit for the influx of terrestrial sediment into the submarine cave from regional storminess.

Late Holocene $\delta^{18}\text{O}_f$ values on *Trilocolina oblonga* tests indicate that late Holocene thermal variability in Walsingham Cavern, and by corollary the adjacent coastal oceans, is linked to proxy-based evidence from elsewhere of NAO phasing. More specifically, Walsingham Cavern cooled by ~1°C at ~2400 cal years B.P. and from 700 cal years B.P. to present, which are within uncertainties of prominent NAO⁻ shifts (Figure 9g). These thermal correlations are consistent with previous high-resolution coral reconstructions from Bermuda [Pätzold *et al.*, 1999; Draschba *et al.*, 2000; Kuhnert *et al.*, 2005; Goodkin *et al.*, 2008a, 2008b], where NAO⁻ (NAO⁺) cause regional cooling (warming) events. No salient temperature change was observed at ~1700 cal years B.P., at which time there is also little evidence in proxy records from Greenland for a prominent NAO phase shift.

In contrast, the influx of terrestrial sediment into Walsingham Cavern from storm-mediated erosion was concentrated during three periods: prior to 3100 cal years B.P., 1300 to 1800 cal years B.P., and during the LIA (700 to 100 cal years B.P.). However, the precise meteorological driver of these storm periods remains uncertain because they occur simultaneous with evidence for both elevated tropical and possible extratropical cyclone activity (Figure 10). Higher-resolution and calibrated hurricane records are required from Bermuda to disentangle the precise meteorological driver of the Walsingham Cavern storminess signal, but the results cast doubt that the low-frequency storminess signal in the North Atlantic can be interpreted in terms of just extratropical storm variability.

Nevertheless, the terrestrial erosion into Walsingham Cavern provides a previously unknown storminess signal for the Bermudian region and an important clue for understanding the low-frequency storminess signal observed throughout the North Atlantic Ocean. Despite the role of NAO phasing on modern North Atlantic storminess [Andrade *et al.*, 2008; Hurrell and Deser, 2009] and Bermuda's climate, the three intervals of storminess documented at Walsingham Cavern are more closely linked with North Atlantic cooling events during the late Holocene that are possibly linked to subtle AMOC forcing.

References

- Airoidi, L., and F. Cinelli (1996), Variability of fluxes of particulate material in a submarine cave with chemolithoautotrophic inputs of organic carbon, *Mar. Ecol. Prog. Ser.*, 139(1–3), 205–217.
- Andrade, C., R. M. Trigo, M. C. Freitas, M. C. Gallego, P. Borges, and A. M. Ramos (2008), Comparing historic records of storm frequency and the North Atlantic Oscillation (NAO) chronology for the Azores region, *Holocene*, 18(5), 745–754.
- Beddows, P. A., P. L. Smart, F. F. Whitaker, and S. L. Smith (2005), Density stratified groundwater circulation on the Caribbean coast of Yucatan Peninsula, Mexico, in *Hydrogeology and Biology of Post-Paleozoic Carbonate Aquifers*, *Spec. Publ.*, vol. 7, edited by J. B. Martin, C. M. Wicks, and I. D. Sasowsky, pp. 129–134, Karst Waters Institute, Charles Town, W. Va.

Acknowledgments

Field support for this project was provided by the Williams and Nolan Families and the Walsingham Land Trust, and data support from the Bermuda Weather Service and R. Johnson (BIOS). This manuscript benefited from discussions with L. Keigwin and B. Curry, and insightful reviews completed by P. Sabatier and two anonymous reviewers. Awards from the National Sciences and Engineering Research Council of Canada (Alexander Graham Bell CGS and Post-Doctoral Fellowship) and the inaugural Johanna M. Resig Fellowship from the Cushman Foundation for Foraminiferal Research provided primary research support, along with research grants from the Geologic Society of America, Cave Research Foundation, the Bermuda Zoological Society, WHOI Ocean and Climate Change Institute, and in part funded by the NSF Division of Ocean Sciences (Award #1519557). This research was conducted under the support of T. Trott and A. Pettit with Bermuda Department of Environmental Protection Permit grants SP081103 and 11101. Data for this project will be made publicly available through the NOAA National Climatic Data Center (www.ncdc.noaa.gov/data-access/paleoclimatology-data/datasets).

- Beddows, P. A., P. L. Smart, F. F. Whitaker, and S. Smith (2007), Decoupled fresh-saline groundwater circulation of a coastal carbonate aquifer: Spatial patterns of temperature and specific conductivity, *J. Hydrol.*, *346*, 18–22.
- Bemis, B. E., H. J. Spero, J. Bijima, and D. W. Lea (1998), Reevaluation of the oxygen isotopic composition of planktonic foraminifera: Experimental results and revised paleotemperature equation, *Paleoceanography*, *13*(2), 150–160, doi:10.1029/98PA00070.
- Bianchi, G. G., and I. N. McCave (1999), Holocene periodicity in North Atlantic climate and deep-ocean flow south of Iceland, *Nature*, *397*, 515–517.
- Blaauw, M., and A. Christen (2011), Flexible paleoclimate age-depth models using an autoregressive gamma process, *Bayesian Anal.*, *6*(3), 457–474.
- Blockley, S. P. E., M. Blaauw, C. Bronk Ramsey, and J. van der Plicht (2007), Building and testing age models for radiocarbon dates in Lateglacial and early Holocene sediments, *Quat. Sci. Rev.*, *26*(15–16), 1915–1926.
- Blockley, S. P. E., C. Ramsey, C. Lane, and A. Lotter (2008), Improved age modelling approaches as exemplified by the revised chronology for the Central European varved lake Soppensee, *Quat. Sci. Rev.*, *27*(1–2), 61–71.
- Bond, G., W. Showers, M. Cheseby, R. Lotti, P. Almasi, P. deMenocal, P. Priore, H. Cullen, I. Hajdas, and I. Bonani (1997), A pervasive millennial-scale cycle in North Atlantic Holocene and glacial climates, *Science*, *278*, 1257–1266.
- Bond, G., B. Kromer, J. Beer, R. Muscheler, M. N. Evans, W. Showers, S. Hoffmann, R. Lotti-Bond, I. Hajdas, and I. Bonani (2001), Persistent solar influence on the North Atlantic climate during the Holocene, *Science*, *294*(2130), 2130–2136.
- Brandon, C., J. D. Woodruff, P. Lane, and J. P. Donnelly (2013), Constraining flooding conditions for prehistoric hurricanes from resultant deposits preserved in Florida sinkholes, *Geophys. Geosyst.*, *14*, 2993–3008, doi:10.1002/ggge.20217.
- Bronk Ramsey, C. (2008), Deposition models for chronological records, *Quat. Sci. Rev.*, *27*(1–2), 42–60.
- Clarke, M., H. Rendell, J.-P. Tastet, B. Clave, and L. Masse (2002), Late-Holocene sand invasion and North Atlantic storminess along the Aquitaine Coast, southwest France, *Holocene*, *12*, 231–238.
- Cordero, R. R., H. Panarello, S. Lanzelotti, and C. M. Favier Dubois (2003), Radiocarbon age offsets between living organisms from the marine and continental reservoir in coastal localities from Patagonian (Argentina), *Radiocarbon*, *45*(1), 9–15.
- Corriero, G., L. S. Liaci, D. Ruggiero, and M. Pansini (2001), The sponge community of a semi-submerged Mediterranean Cave, *Mar. Ecol. Prog. Ser.*, *21*(1), 85–96.
- Craig, H. (1957), Isotopic standards for carbon and oxygen and correction factors for mass-spectrometric analysis of carbon dioxide, *Geochim. Cosmochim. Acta*, *12*, 133–149.
- Cronin, T. M., K. Hayo, R. C. Thunell, G. S. Dwyer, C. Saenger, and D. A. Willard (2010), The Medieval Climate Anomaly and the Little Ice Age in Chesapeake Bay and the North Atlantic Ocean, *Palaeogeogr. Palaeoclimatol. Palaeoecol.*, *297*, 299–310.
- Cunliffe, S. (1985), The flora and fauna of Sagittarius, an anchialine cave and lake in Grand Bahama, *Cave Sci.*, *12*(3), 103–109.
- Dawson, A. G., L. Elliot, P. Mayewski, P. Lockett, S. Noone, K. Hickey, and T. Holt (2003), Late-Holocene North Atlantic climate ‘seesaws’, storminess changes and Greenland ice sheet (GISP2) palaeoclimates, *Holocene*, *13*, 381–392.
- de Jong, R., S. Björck, L. Björkman, and L. B. Clemmensen (2006), Storminess variation during the last 6500 years as reconstructed from an ombrotropic peat bog in Halland, southwest Sweden, *J. Quat. Sci.*, *21*, 905–919.
- deMenocal, P., J. Ortiz, T. Guilderson, and M. Sarnthein (2000), Coherent high- and low-latitude climate variability during the Holocene Warm Period, *Science*, *288*, 2198–2202.
- Denomee, K. C., S. J. Bentley, and A. W. Droxler (2014), Climatic control on hurricane patterns: A 1200-year near-annual record from Lighthouse Reef, Belize, *Sci. Rep.*, *4*(3876), 7.
- Denton, G. H., and W. Karlén (1973), Holocene climatic variations—Their pattern and possible cause, *Quat. Res.*, *3*(2), 155–174.
- Dodge, R. E., and J. R. Vaišnyš (1975), Hermatypic coral growth banding as environmental recorder, *Nature*, *238*, 706–708.
- Donnelly, J. P., and J. D. Woodruff (2007), Intense hurricane activity over the past 5,000 years controlled by El Niño and the West African Monsoon, *Nature*, *447*, 465–468.
- Donnelly, J. P., et al. (2001), 700 year sedimentary record of intense hurricane landfalls in southern New England, *Geol. Soc. Am. Bull.*, *113*, 715–727.
- Donnelly, J. P., A. D. Hawkes, P. Lane, D. MacDonald, B. N. Shuman, M. R. Toomey, P. J. van Hengstum, and J. D. Woodruff (2015), Climate forcing of unprecedented intense-Hurricane activity in the last 2,000 years, *Earth’s Future*, in press.
- Draschba, S., J. Pätzold, and G. Wefer (2000), North Atlantic climate variability since AD 1350 recorded in $\delta^{18}\text{O}$ and skeletal density of Bermuda corals, *Int. J. Earth Sci.*, *88*, 733–741.
- Druffel, E. R. M. (1997), Pulses of rapid ventilation in the North Atlantic surface ocean during the past century, *Science*, *275*, 1454–1457.
- Dutton, A., E. Bard, F. Antonioli, T. M. Esat, K. Lambeck, and M. T. McCulloch (2009), Phasing and amplitude of sea-level and climate change during the penultimate interglacial, *Nat. Geosci.*, *2*, 355–359.
- Eshel, G., G. J. Levy, U. Mingelgrin, and M. J. Singer (2004), Critical evaluation of the use of laser diffraction for particle-size distributions analysis, *Soil Sci. Soc. Am. J.*, *68*, 736–743.
- Gili, J. M., T. Riera, and M. Zabala (1986), Physical and biological gradients in a submarine cave on the Western Mediterranean coast (north-east Spain), *Mar. Biol.*, *90*, 291–297.
- Goodkin, N. F., K. A. Hughen, W. B. Curry, and S. C. Doney (2008a), Sea Surface temperature and salinity variability at Bermuda during the end of the Little Ice Age, *Paleoceanography*, *23*, PA3203, doi:10.1029/2007PA001532.
- Goodkin, N. F., K. A. Hughen, S. C. Doney, and W. B. Curry (2008b), Increased multidecadal variability of the North Atlantic Oscillation since 1781, *Nat. Geosci.*, *1*, 844–848.
- Guichard, M. P., E. A. Nelson, J. L. Evans, and D. G. O’Connell (2007), Bermuda subtropical storms, *Meteorol. Atmos. Phys.*, *97*, 239–253.
- Hall, I. R., G. G. Bianchi, and J. R. Evans (2004), Centennial to millennial scale Holocene climate–deep water linkage in the North Atlantic, *Quat. Sci. Rev.*, *23*, 1529–1536.
- Harmon, R. S., H. P. Schwarcz, and D. C. Ford (1978), Late Pleistocene sea level history of Bermuda, *Quat. Res.*, *9*, 205–218.
- Heiri, O., A. F. Lotter, and G. Lemcke (2001), Loss on ignition as a method for estimating organic and carbonate content in sediments: Reproducibility and comparability of results, *J. Paleolimnol.*, *25*, 101–110.
- Horton, B. P., V. Rossi, and A. D. Hawkes (2009), The sedimentary record of the 2005 hurricane season from the Mississippi and Alabama coastlines, *Quat. Int.*, *195*, 15–30.
- Hurrell, J. W., and C. Deser (2009), North Atlantic climate variability: The role of the North Atlantic Oscillation, *J. Mar. Syst.*, *78*, 28–41.
- Jackson, M. G., N. Oskarsson, R. G. Trønnes, J. F. McManus, D. W. Oppo, K. Gronvold, S. R. Hart, and J. P. Sachs (2005), Holocene loess deposition in Iceland: Evidence for millennial-scale atmosphere-ocean coupling in the North Atlantic, *Geology*, *33*(6), 509–512.
- Jelgersma, S., M. J. F. Stive, and L. van der Valk (1995), Holocene storm surge signatures in the coastal dunes of the western Netherlands, *Mar. Geol.*, *125*, 95–110.

- Jones, C. S., et al. (2003), The extratropical transition of tropical cyclones: Forecast challenges, current understanding, and future directions, *Weather Forecasting*, 18, 1052–1092.
- Kano, Y., and T. Kase (2008), Diversity and distribution of the submarine-cave Neritiliidae in the Indo-Pacific (Gastropoda: Neritimorpha), *Org. Diversity Evol.*, 8, 22–43.
- Katz, M. E., B. S. Cramer, A. Franzese, B. Hönisch, K. G. Miller, Y. Rosenthal, and J. D. Wright (2010), Traditional and emerging geochemical proxies in foraminifera, *J. Foraminiferal Res.*, 40(2), 165–192.
- Keigwin, L. D. (1996), The little ice age and medieval warm period in the Sargasso Sea, *Science*, 274(5292), 1504–1508.
- Keigwin, L. D., and G. A. Jones (1994), Western North Atlantic evidence for millennial-scale changes in ocean circulation and climate, *J. Geophys. Res.*, 99, 12,397–12,410, doi:10.1029/94JC00525.
- Kim, S. T., and J. R. O'Neil (1997), Equilibrium and nonequilibrium oxygen isotope effects in synthetic carbonates, *Geochim. Cosmochim. Acta*, 61(12), 3461–3475.
- Kitamura, A., et al. (2007), Potential of submarine-cave sediments and oxygen isotope composition of cavernicolous micro-bivalve as a late Holocene paleoenvironmental record, *Global Planet. Change*, 55(4), 301–316.
- Koblunk, D. R., and M. A. Lysenko (1986), Reef-dwelling molluscs in open framework cavities Bonaire, N.A., and their potential for preservation in a fossil reef, *Bull. Mar. Sci.*, 39(3), 656–672.
- Kossin, J. P., S. J. Camargo, and M. Sitkowski (2010), Climate modulation of North Atlantic hurricane tracks, *J. Clim.*, 23, 3057–3076.
- Kuhn, G. (1984), Sedimentations-geschichte der Bermuda North Lagoon im Holozän, PhD thesis, 272 pp., Universität zu Göttingen.
- Kuhnert, H., T. Crüger, and J. Pätzold (2005), NAO signature in a Bermuda coral Sr/Ca record, *Geochem. Geophys. Geosyst.*, 6, Q04004, doi:10.1029/2004GC000786.
- Land, L. S., F. T. Mackenzie, and S. J. Gould (1967), The Pleistocene history of Bermuda, *GSA Bull.*, 78, 993–1006.
- Lane, P., J. P. Donnelly, J. D. Woodruff, and A. D. Hawkes (2011), A decadal-resolved paleohurricane record archived in the late Holocene sediments of a Florida sinkhole, *Mar. Geol.*, 287, 14–30.
- Logan, A., S. M. Mathers, and M. L. H. Thomas (1984), Sessile invertebrate coelobite communities from reefs of Bermuda: Species composition and distribution, *Coral Reefs*, 2, 205–213.
- Logan, A., L. Yang, and T. Tomascik (1994), Linear skeletal extension rates in two species of *Diplora* from high-latitude reefs in Bermuda, *Coral Reefs*, 13, 225–230.
- Lund, D. C., and W. B. Curry (2004), Late Holocene variability in Florida Current surface density: Patterns and possible causes, *Paleoceanography*, 19, PA4001, doi:10.1029/2004PA001008.
- Lund, D. C., J. Lynch-Stieglitz, and W. B. Curry (2006), Gulf Stream density structure and transport during the past millennium, *Nature*, 444(30), 601–604.
- Luter, C., G. Worheide, and J. Reitner (2003), A new thecideid genus and species (Brachiopoda, Recent) from submarine caves of Osprey Reef (Queensland Plateau, Coral Sea, Australia), *J. Nat. Hist.*, 37(12), 1423–1432.
- Maddocks, R. F., and T. M. Illiffe (1986), Podocopid ostracoda of Bermudian caves, *Stylogologia*, 2(1/2), 26–76.
- Mailier, P. J., D. B. Stephenson, C. A. T. Ferro, and K. I. Hodges (2006), Serial clustering of extratropical cyclones, *Mon. Weather Rev.*, 134, 2224–2240.
- Martin, J. B., J. Gulley, and P. Spellman (2012), Tidal pumping of water between Bahamian blue holes, aquifers, and the ocean, *J. Hydrol.*, 416–417, 28–38.
- Mauquoy, D., B. van Geel, M. Blaauw, and J. van der Plicht (2002), Evidence from northwest European bogs shows 'Little Ice Age' climatic changes driven by variations in solar activity, *Holocene*, 12, 1–6.
- Mayewski, P. A., et al. (2004), Holocene climate variability, *Quat. Res.*, 62, 243–255.
- McIntyre, C. P., M. L. Roberts, J. R. Burton, A. P. McNichol, A. Burke, L. F. Robinson, K. F. von Reden, and W. J. Jenkins (2011), Rapid radiocarbon (^{14}C) analysis of coral and carbonate samples using a continuous flow accelerator mass spectrometry CFAMS system, *Paleoceanography*, 26, PA4212, doi:10.1029/2011PA002174.
- Moore, Y. H., R. K. Sotessell, and D. H. Easley (1992), Fresh-water/sea-water relationship within a ground-water flow system, northeastern coast of the Yucatan Peninsula, *Ground Water*, 30(3), 343–350.
- Morberg, A., D. M. Sonechkin, K. Holmgren, N. M. Datsenko, and W. Karlén (2005), Highly variable Northern Hemisphere temperatures reconstructed from low- and high-resolution proxy data, *Nature*, 433, 613–617.
- Morris, B., J. Barnes, F. Brown, and J. Markham (1977), *The Bermuda Marine Environment: A Report of the Bermuda Inshore Waters Investigations 1976–1977*, Spec. Publ., vol. 15, 120 pp., Bermuda Biological Station, St. Georges, Bermuda.
- Mylroie, J. E., J. L. Carew, and H. L. Vacher (1995), Karst development in the Bahamas and Bermuda, in *Terrestrial and Shallow Marine Geology of the Bahamas and Bermuda*, edited by H. A. Curran and B. White, *Geol. Soc. Am. Spec. Pap.*, 300, 251–267.
- Mylroie, J. R., and J. E. Mylroie (2007), Development of the carbonate island karst model, *J. Cave Karst Stud.*, 69(1), 59–75.
- Noren, A. J., P. R. Bierman, E. J. Steig, A. Lini, and J. Southon (2002), Millennial-scale storminess variability in the northeastern United States during the Holocene epoch, *Nature*, 419, 821–824.
- O'Brien, S. R., P. A. Mayewski, L. D. Meeker, D. A. Meese, M. S. Twickler, and S. I. Whitlow (1995), Complexity of Holocene climate as reconstructed from a Greenland Ice Core, *Science*, 270(5244), 1962–1964.
- Ohtsuka, S., T. Kase, and G. A. Boxshall (2000), A new species of Ridgewayia (Copepoda: Calanoida) from a submarine cave in Palau, western Pacific, *Species Diversity*, 5, 201–213.
- Ohtsuka, S., Y. Hanamura, and T. Kase (2002), A new species of Thetispelecaris (Crustacea: Peracarida) from submarine cave on Grand Cayman Island, *Zool. Sci.*, 19, 611–624.
- Olsen, J., N. J. Anderson, and M. F. Knudsen (2012), Variability of the North Atlantic Oscillation over the past 5,200 years, *Nat. Geosci.*, 5, 808–812.
- Omori, A., A. Kitamura, K. Fujita, K. Honda, and N. Yamamoto (2010), Reconstruction of light conditions within a submarine cave during the past 7000 years based on the temporal and spatial distribution of algal symbiont-bearing large benthic foraminifers, *Palaeogeogr. Palaeoclimatol. Palaeoecol.*, 292, 443–452.
- Oppo, D. W., J. F. McManus, and J. L. Cullen (2003), Deep water variability in the Holocene epoch, *Nature*, 422, 277–278.
- Ortiz, M., J. M. Guerra-García, and R. Lalana (2009), *Cubadeutella cavernicola*: A new genus and species of Caprellidae (Crustacea: Amphipoda) from Cuba, *Zootaxa*, 2130, 60–68.
- Palmer, A. N., M. V. Palmer, and J. M. Queen (1977), Geology and origin of the caves of Bermuda, in *Proceedings of the Seventh International Congress of Speleology*, pp. 336–339, British Cave Research Association, Sheffield, U. K.
- Park, L. E. (2012), Comparing two long-term hurricane frequency and intensity records from San Salvador Island, Bahamas, *J. Coastal Res.*, 28, 891–902.

- Patterson, W. P., K. A. Dietrich, C. Holmden, and J. T. Andrews (2010), Two millennia of North Atlantic Seasonality and implications for Norse colonies, *Proc. Natl. Acad. Sci. U.S.A.*, *107*(12), 5306–5310, doi:10.1073/pnas.0902522107.
- Pätzold, J., T. Bickert, B. Flemming, H. Grobe, and G. Wefer (1999), Holozänes Klima des Nordatlantiks rekonstruiert aus massiven Korallen von Bermuda, *Nat. Mus.*, *129*, 165–177.
- Rasmussen, K. A., and C. E. Brett (1985), Taphonomy of Holocene cryptic biots from St. Croix, Virgin Islands: Information loss and preservational biases, *Geology*, *13*, 551–553.
- Reimer, P. J., et al. (2013), IntCal13 and Marine13 radiocarbon age calibration curves 0–50,000 years Cal BP, *Radiocarbon*, *55*(4), 1869–1887.
- Renssen, H., H. Goose, and T. Fichefet (2007), Simulation of Holocene cooling events in a coupled climate model, *Quat. Sci. Rev.*, *26*, 2019–2029.
- Richards, D. A., P. L. Smart, and R. L. Edwards (1994), Maximum sea levels for the last glacial period from U-series ages of submerged speleothems, *Nature*, *367*, 357–360.
- Roberts, M. L., K. F. von Reden, J. R. Burton, C. P. McIntyre, and S. R. Beaupré (2013), A gas-accepting ion source for Accelerator Mass Spectrometry: Progress and applications, *Nucl. Instrum. Methods Phys. Res. B*, *294*, 296–299.
- Rueger, B. F. (2006), Late Holocene vegetation and fire history of Devonshire Marsh, Bermuda, 5000 yBP to present, in *Proceedings of the 12th Symposium on the Geology of the Bahamas and Other Carbonate Regions*, edited by R. L. Davis and D. W. Gamble, pp. 162–178, Gerace Research Center, San Salvador, Bahamas.
- Rueger, B. F., and T. N. von Wallmenich (1996), Human impact on the forests of Bermuda: The decline of endemic cedar and palmetto since 1609, recorded in Holocene pollen record of Devonshire Marsh, *J. Paleolimnol.*, *16*, 59–66.
- Ruprecht, E., S. S. Schroeder, and S. Ubl (2002), On the relation between NAO and water vapour transport towards Europe, *Meteorol. Z.*, *11*(6), 365–401.
- Sabatier, P., L. Dezileau, P. Blanchemanche, G. Siani, M. Condomines, I. Bentaleb, and G. Piques (2010), Holocene variations of radiocarbon reservoir ages in a Mediterranean lagoonal system, *Radiocarbon*, *52*(1), 1–12.
- Sabatier, P., L. Dezileau, C. Colin, L. Briquieu, F. Bouchette, P. Martinez, G. Siani, O. Raynal, and U. Von Grafenstein (2012), 7000 years of paleostorm activity in the NW Mediterranean Sea in response to Holocene climate events 7000 years of paleostorm activity in the NW Mediterranean Sea in response to Holocene climate events, *Quat. Res.*, *77*, 1–11.
- Saenger, C., R. E. Came, D. W. Oppo, L. D. Keigwin, and A. L. Cohen (2011), Regional climate variability in the western subtropical North Atlantic during the past two millennia, *Paleocyanography*, *26*, PA2206, doi:10.1029/2010PA002038.
- Schroeder, E. S., H. Stommel, W. Menzel, and W. J. Sutcliffe (1959), Climatic stability of eighteen degree water at Bermuda, *J. Geophys. Res.*, *64*(3), 363–366, doi:10.1029/JZ064i003p00363.
- Shaffrey, L., and R. Sutton (2006), Bjerknes compensation and the decadal variability of the energy transports in a coupled climate model, *J. Clim.*, *19*, 1167–1181.
- Sket, B., and T. M. Iliffe (1980), Cave fauna of Bermuda, *Int. Rev. Gesmten Hydrobiol.*, *65*, 871–882.
- Smart, C. C. (1984), The hydrology of the inland blue holes, Andros Island, *Cave Sci.*, *11*(1), 23–29.
- Sorrel, P., B. Tessier, F. Demory, N. Delsinne, and D. Mouazé (2009), Evidence for millennial-scale climatic events in the sedimentary infilling of a macrotidal estuarine system, the Seine estuary (NW France), *Quat. Sci. Rev.*, *28*(5–6), 499–516.
- Sorrel, P., M. Debret, I. Billeaud, S. L. Jaccard, J. F. McManus, and B. Tessier (2012), Persistent non-solar forcing of Holocene storm dynamics in coastal sedimentary archives, *Nat. Geosci.*, *5*, 892–896.
- Spalding, R. F., and T. D. Matthews (1972), Submerged stalagmites from caves in the Bahamas: Indicators of low sea level stand, *Quat. Res.*, *2*(4), 470–472.
- Surić, M., D. A. Richards, D. L. Hoffmann, D. Tibiljaš, and M. Juračić (2009), Sea-level change during MIS 5a based on submerged speleothems from the eastern Adriatic Sea (Croatia), *Mar. Geol.*, *262*(1–4), 62–67.
- Swindles, G. T., G. Plunkett, and H. M. Roe (2007), A delayed climatic response to solar forcing at 2800 cal BP: Multiproxy evidence from three Irish peatlands, *Holocene*, *17*(2), 177–182.
- Tabuki, R., and T. Hanai (1999), A new sigillid ostracod from the submarine caves of the Ryukyu islands, Japan, *Palaeontology*, *42*(4), 569–593.
- Thornalley, D. J. R., H. Elderfield, and I. N. McCave (2009), Holocene oscillations in temperature and salinity of the surface subpolar North Atlantic, *Nature*, *457*, 711–714.
- Toomey, M. R., W. B. Curry, J. P. Donnelly, and P. J. van Hengstum (2013), Reconstructing 7000 years of North Atlantic hurricane variability using deep-sea sediment cores from the western Great Bahama Bank, *Paleocyanography*, *28*, 31–41, doi:10.1002/palo.20012.
- Trouet, V., J. Esper, N. E. Graham, A. Baker, J. D. Scourse, and D. C. Frank (2009), Persistent positive North Atlantic Oscillations mode dominated the medieval climate anomaly, *Science*, *324*, 78–80.
- Vacelet, J. (1996), Deep-sea sponges in a Mediterranean cave, in *Deep-Sea and Extreme Shallow-Water Habitats: Affinities and Adaptations*, *Biosyst. Ecol. Ser.*, vol. 11, edited by F. Uiblein, J. Ott, and M. Stachowitsch, pp. 299–312, Österreichische Akademie der Wissenschaften, Vienna.
- Vacher, H. L., and P. J. Hearty (1989), History of stage 5 sea level in Bermuda: Review with new evidence of a brief rise to present sea level during substage 5a, *Quat. Sci. Rev.*, *8*, 159–168.
- Vacher, H. L., P. J. Hearty, and M. P. Rowe (1995), Stratigraphy of Bermuda: Nomenclature, concepts, and status of multiple systems of classification, in *Terrestrial and Shallow Marine Geology of the Bahamas and Bermuda*, edited by H. A. Curran and B. White, *Geol. Soc. Am. Spec. Pap.*, *300*, 271–294.
- van Geel, B., C. J. Heusser, H. Renssen, and C. J. E. Schuurmans (2000), Climatic change in Chile at around 2700 BP and global evidence for solar forcing: A hypothesis, *Holocene*, *10*, 659–664.
- van Geel, B., H. Heijnis, D. J. Charman, G. Thompson, and S. Engels (2014), Bog burst in the eastern Netherlands triggered by the 2.8 kyr BP climate event, *Holocene*, *24*(11), 1465–1477, doi:10.1177/0959683614544066.
- van Hengstum, P. (2010), Quaternary sea-level and climate signatures in phreatic coastal caves, PhD thesis, 299 pp., Dalhousie Univ., Halifax, U. K.
- van Hengstum, P. J., and D. B. Scott (2011), Ecology of foraminifera and habitat variability in an underwater cave: Distinguishing anchialine versus submarine cave environments, *J. Foraminiferal Res.*, *41*(3), 201–229.
- van Hengstum, P. J., E. G. Reinhardt, P. A. Beddows, H. P. Schwarcz, and J. J. Garbriel (2009), Foraminifera and testate amoebae (thecamoebians) in an anchialine cave: Surface distributions from Aktun Ha (Carwash) cave system, Mexico, *Limnol. Oceanogr.*, *54*(1), 391–396.
- van Hengstum, P. J., D. B. Scott, D. R. Gröcke, and M. A. Charette (2011), Sea level controls sedimentation and environments in coastal caves and sinkholes, *Mar. Geol.*, *286*, 35–50.
- van Hengstum, P. J., J. P. Donnelly, M. R. Toomey, N. A. Albury, P. Lane, and B. Kakuk (2014), Heightened hurricane activity on the Little Bahama Bank from 1350 to 1650 AD, *Cont. Shelf Res.*, *86*, 103–115.
- van Hengstum, P. J., D. A. Richards, B. P. Onac, and J. A. Dorale (2015), Coastal caves and sinkholes, in *Handbook of Sea-Level Research*, edited by I. Shennan, A. J. Long, and B. P. Horton, p. 836, John Wiley, Hoboken, N. J.

- Vollbrecht, R. (1996), *Postglazialer Anstieg des Meeresspiegels, Paläoklima und Hydrographie, Aufgezeichnet in Sedimenten der Bermuda Inshore Waters*, 383 pp., Universität Göttingen, Göttingen, Germany.
- Watts, W. A., and B. C. S. Hansen (1986), Holocene climate and vegetation of Bermuda, *Pollen Spores*, 28(3–4), 355–364.
- Whitaker, F. F., and P. L. Smart (1990), Active circulation of saline ground waters in carbonate platforms: Evidence from the Great Bahama Bank, *Geology*, 18, 200–203.
- Wilson, P., J. M. McGourty, and M. D. Bateman (2004), Mid- to late-Holocene coastal dune stratigraphy for the north coast of Northern Ireland, *Holocene*, 14, 406–416.
- Yamamoto, N., A. Kitamura, T. Irino, T. Kase, and S. Ohashi (2008), Reconstruction of paleotemperatures in the Northwest Pacific over the past 3000 years from $\delta^{18}\text{O}$ values of the micro-bivalvia *Carditella iejimensis* found in a submarine cave, *Global Planet. Change*, 62, 97–108.
- Yamamoto, N., A. Kitamura, A. Ohmori, Y. Morishima, T. Toyofuku, and S. Ohashi (2009), Long-term changes in sediment type and cavernicolous bivalve assemblages in Daidokutsu submarine cave, Okinawa Islands: Evidence from a new core extending over the past 7,000 years, *Coral Reefs*, 28, 967–976.
- Yamamoto, N., A. Kitamura, T. Irino, T. Kase, and S. Ohashi (2010), Climatic and hydrologic variability in the East China Sea during the last 7000 years based on oxygen isotopic records of the submarine cavernicolous micro-bivalve *Carditella iejimensis*, *Global Planet. Change*, 72(3), 131–140.
- Zabala, M., T. Riera, J. M. Gili, M. Barange, A. Lobo, and J. Penuelas (1989), Water flow, trophic depletion, and benthic macrofauna impoverishment in a submarine cave from the western Mediterranean, *Mar. Ecol.*, 10(3), 271–287.